

**MICROWAVE HEATING OF A COATING ON A TEMPERATURE-
SENSITIVE SUBSTRATE**

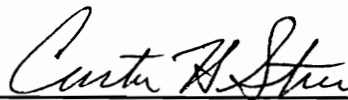
by

Daniel B. Skinner

Thesis submitted to the Faculty of the
Virginia Polytechnic Institute and State University

MASTERS OF SCIENCE
IN
MECHANICAL ENGINEERING

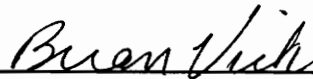
APPROVED:



Curtis H. Stern, Chairman



Elaine P. Scott



Brian Vick

November 20, 1995
Blacksburg, Virginia

c.2

LD
5655
V855
1995
S555
C.2

MICROWAVE HEATING OF A COATING ON A TEMPERATURE-SENSITIVE SUBSTRATE

by

Daniel B. Skinner

Dr. Curtis H. Stern, Chairman

Mechanical Engineering

(ABSTRACT)

Microwave heating has been considered for the heating of a coating in contact with a temperature-sensitive substrate. A methodology was developed to conduct a microwave heating feasibility study for a candidate system. The study consisted of dielectric property determination, development of heat transfer models to determine the heat generation rates necessary to achieve a desired temperature distribution, calculation of the required electric field strength given the dielectric properties and heat generation rates, and examination of whether the microwave heating could be performed with available equipment. Sol-gel processing of a 1 μm -thick boehmite coating on a non-woven polypropylene substrate was chosen as the candidate system. It was desired to selectively heat the boehmite to 250° C without damaging the polypropylene, which degrades at 150° C. Dielectric measurements indicated that the boehmite could be heated to 250° C using microwave energy. Microwave heating of the system was then modeled using three techniques: an approximate analytical solution based on Composite Green's Functions, a finite difference solution, and an approximate lumped capacitance solution. It was determined that the heat generation rates necessary to produce the desired temperature distribution would require field strengths beyond practical limitations for the specific boehmite-polypropylene system considered.

Acknowledgments

I would like to thank the following people for their help and guidance while conducting this research:

Dr. Curtis H. Stern, for all of his assistance, patience, guidance, and generosity. I am very grateful for all that he has done, especially for always having his door open and for helping me to see the positive in every research setback. The confidence I've developed in my technical abilities is a direct result of his support.

To Kimberly-Clark and Dennis Everhart, for the impetus and funding for this research.

To Dr. Elaine Scott and Dr. Brian Vick, for serving on my committee and for the suggestions they made. To Dr. Vick I am especially grateful for the appreciation of mathematics and Green's functions that he fostered in me through his teaching. My class 'project' became an large and enjoyable portion of my research effort.

To Dr. J. Graybeal, Chemistry Department, for the generous use of the HP Network Analyzer System.

To my parents, Dr. Charles K. and Helen C. Skinner, for their love, support, and encouragement in helping to reach this point in my life. Dad, thanks for always wanting the best for me and for pushing me towards my long-term goals. Mom, thanks for doing all those little things which mean so much.

To Jori, for becoming such a special part of my life. Thank you for your love and patience during this endeavor. As I embark on the rest of my life, I can think of no better person to make the journey with. I am so proud of you. Love and thanks always.

Table of Contents

List of Tables.....	vi
List of Figures.....	vii
Nomenclature	ix
1. Introduction	1
1.1 Microwave Heating Feasibility Study Requirements	2
1.2 Microwave Sol-Gel Processing of a Boehmite/ Polypropylene System.....	4
1.3 Literature Review.....	8
1.4 Objectives.....	10
1.5 Overview.....	10
2. Theoretical Overview of Microwave Heating.....	13
2.1 Polarization.....	13
2.2 Complex Permittivity	15
2.3 Volumetric Heat Dissipation.....	16
3. Experimental Procedures and Results.....	20
3.1 Dielectric Property Determination.....	20
3.1.1 Sample Preparation.....	21
3.1.2 Dielectric Testing Using the Cavity Perturbation Technique.....	21
3.1.2.1 Background	21
3.1.2.2 Equipment.....	23
3.1.2.3 Test Procedure	25
3.1.3 Results.....	26
3.2 Microwave Heating of Boehmite Sol-Gel.....	30
3.2.1 Sample Preparation.....	30
3.2.2 Microwave Heating of Boehmite Using a Multimode Microwave Oven.....	31
3.2.2.1 Background	31
3.2.2.2 Equipment.....	33
3.2.2.3 Procedure.....	36
3.2.3 Results.....	38
3.3 Microwave Heating of a Boehmite Sol Coating on a Polypropylene Nonwoven.....	38
3.3.1 Calorimetry Studies of the Electric Field Strength	39
3.3.2 Sample Preparation.....	41
3.3.3 Equipment.....	42
3.3.4 Results.....	42
4. Heat Transfer Modeling	44
4.1 Model Description	44
4.2 Approximate Analytical Green's Function Solution.....	46
4.2.1 Governing Equations.....	46
4.2.2 Spatial Boundary Conditions.....	47
4.2.3 Initial Conditions.....	48

4.2.4	Solution Assumptions	48
4.2.5	Green's Function Solution	48
4.2.5.1	Eigenvalue Determination.....	49
4.2.5.2	Transient Temperature Distribution Determination.....	51
4.3	Finite Difference Solution	52
4.3.1	Governing Equations.....	52
4.3.2	Spatial Boundary Conditions.....	53
4.3.3	Initial Conditions.....	54
4.3.4	Solution Assumptions.....	54
4.3.5	Finite Difference Solution Nodal Equations	54
4.3.5.1	Center Node - Node 1	55
4.3.5.2	Internal Node i, Layer 1 (polypropylene).....	56
4.3.5.3	Interface Node M.....	56
4.3.5.4	Internal Node I, Layer 2 (boehmite).....	57
4.3.5.5	Convection Surface, Node N	57
4.4	Approximate Lumped Capacitance Method.....	58
5.	Validation of the Approximate Analytical Solution.....	61
5.1	Initial Condition Analysis	62
5.2	Heat Generation Analysis.....	64
5.2.1	Approximate Analytical Model and Cartesian Steady State Solution Comparison	67
5.2.2	Approximate Analytical Solution and Cylindrical Solution Comparison.....	67
5.3	Contact Conductance Analysis.....	72
6.	Results of the Heat Transfer Modeling.....	75
6.1	Heat Generation Rate Determination.....	75
6.2	Heat Generation Rate Feasibility.....	78
7.	Conclusions and Recommendations	79
7.1	Conclusions.....	79
7.1.1	Development of a Methodology for a Microwave Heating Feasibility Study	79
7.1.2	Microwave Heating Feasibility Study for the Boehmite/ Polypropylene System.....	81
7.2	Recommendations	82
	References.....	84
	Appendix A: Approximate Analytical Solution - Mathematica Programs.....	125
A.1	Eigenvalue Determination Program.....	125
A.2	Temperature Distribution Determination Program.....	127
A.3	Temperature Distribution Output Program.....	131
	Appendix B: Finite Difference Model - Fortran code.....	134
B.1	Input file - hyp.in	134
B.2	Executable file - hyp.f.....	134
	Vita.....	139

List of Tables

Table 3-1: WR-90 Resonant Cavity Components.....	87
Table 3-2: Dielectric Properties of Selected Materials at Microwave Frequencies.....	88
Table 5-1: Dimensional Values for Test Cases.....	89
Table 6-1: Material Properties for the Heat Transfer Models.....	90
Table 6-2: Model Geometry and Interface Conditions Comparison	91
Table 6-3: Comparison of Model Solutions Using $\dot{q}_2''' = 5.5 \times 10^{13} \text{ W/m}^3$	92

List of Figures

Figure 3-1	Schematic of the Hewlett-Packard 8510B Network Analyzer System.....	93
Figure 3-2	Loss Factor (ϵ'') at 9.4 GHz of Boehmite Dried for One Hour in Oven at Temperature T. (ϵ'' measurements made at room temperature).....	94
Figure 3-3	Low-Loss, Teflon, Cylindrical Sample Holder	95
Figure 3-4	Schematic of the Multimode Oven System.....	96
Figure 3-5	Deviation ΔT of Type K Thermocouple Temperature from being a Linear Function of Voltage Output Between 0 and 300° C (0 mV to 12.25 mV).....	97
Figure 3-6	Microwave Heating of Boehmite Sol-Gel. One hour at 260° C.....	98
Figure 3-7	E_{rms} Determination Data. Microwave Heating of Crushed Pyrex Glass at 60 % Power	99
Figure 3-8	Configuration for the Microwave Heating of a Boehmite Coated Nonwoven.....	100
Figure 3-9	Temperature Profile for Microwave Heating of a Boehmite Coated Nonwoven	101
Figure 4-1	Physical Model of Polypropylene Nonwoven with Boehmite Coating	102
Figure 4-2	Geometry for the Long Polypropylene Fiber Coated with Boehmite	103
Figure 4-3	Geometry of the Approximate Analytical Green's Function Solution.....	104
Figure 4-4	Geometry of the Cylindrical Finite Difference Solution.....	105
Figure 4-5	Geometry of the Lumped Capacitance Solution.....	106
Figure 4-6	Finite Difference Model Nodes	107
Figure 5-1	Geometry of Test Case 1	108
Figure 5-2	Test Case 1: Detail of Solutions at $t = 0$	109
Figure 5-3	Test Case 1: Comparison of Solutions to Initial Condition Problem.....	110
Figure 5-4	Geometry of Test Case 2	111
Figure 5-5	Test Case 2: Comparison Between the Temperature Distribution of the Analytical Model at Steady State and Expected Values.....	112
Figure 5-6	Test Case 2: Comparison between Transient Temperature Distributions of the Analytical Model at $x = 0$ and the Ozisik Solution at $r = 0$	113
Figure 5-7	Test Case 2: Comparison between Transient Temperature Distributions of the Analytical Model at $x/L = 1/2$ and the Ozisik Solution at $r/R = 1/2$	114

Figure 5-8 Test Case 2: Comparison between Transient Temperature Distributions of the Analytical Model at $x/L = 1$ and the Ozisik Solution at $r/R = 1$	115
Figure 5-9 Maximum Temperature Error for the Cartesian (Plane Wall) Solution of Test Case 2.....	116
Figure 5-10 Maximum Temperature Error for Cartesian (Plane Wall) Model at Micron Thicknesses.....	117
Figure 5-11: Test Case 3: Temperature Difference at the Interface over Time as a Function of the Contact Conductance h_c	118
Figure 5-12: Maximum Temperature Difference at the Interface as a Function of the Contact Conductance h_c	119
Figure 5-13: Test Case 3: Time to Maximum Interface ΔT as a Function of the Contact Conductance h_c	120
Figure 6-1: Temperature Distribution at $t = 10.6 \mu s$ Using the Approximate Analytical Solution with $h_c = 5000 \text{ W/m}^2 \cdot \text{K}$ (Model A).....	121
Figure 6-2: Temperature Distribution at $16.2 \mu s$ Using the Approximate Analytical Solution with $h_c = \infty$ (Model B).....	122
Figure 6-3 Temperature Distribution at $14.6 \mu s$ Using the Finite Difference Solution (Model C).....	123
Figure 6-4: Bulk Temperature Over Time Using the Lumped Capacitance Solution (Model D).....	124

Nomenclature

c_{p_i}	Specific heat, layer i (J/kg K)
\vec{D}	Total electric charge flux density vector
\vec{D}_0	Electric charge density due to an externally applied electric field
\vec{E}	Electric field
E	Peak electric field strength (V/m)
E_{rms}	Root mean squared value of the electric field (V/m)
f_r	Resonant frequency (Hz)
$F_i(x)$	Initial temperature distribution, layer i , a function of position ($^{\circ}\text{C}$)
h_c	Contact conductance between layers 1 and 2 ($\text{W}/\text{m}^2\text{ }^{\circ}\text{C}$)
h_{∞}	Convection heat transfer coefficient ($\text{W}/\text{m}^2\text{ }^{\circ}\text{C}$)
\vec{H}	Magnetic field
k_i	Thermal conductivity, layer i ($\text{W}/\text{m }^{\circ}\text{C}$)
L_c	Characteristic length (m)
m	Mass (kg)
N_n	Norm
n	Number of terms in series solution
\vec{P}	Polarization field
P_{av}	Average power dissipated in an isotropic material in a uniform electric field (W/m^3)
$\dot{q}_i'''(x,t)$	Internal heat generation, layer i , function of position and time (W/m^3)
q	Dipole charge
Q	Quality factor; $f_r/\Delta f$
r	Radial coordinate describing distance from centerline (m)
t	Time (s)
T_0	Initial temperature ($^{\circ}\text{C}$)
T_{∞}	Ambient temperature ($^{\circ}\text{C}$)
V	Volume (m^3)
x	Coordinate location describing distance from the insulated boundary (m)
x_i	Distance between the positive and negative charges within a dipole
α_i	Thermal diffusivity, layer i (m^2/s)
β_n	Eigenvalue
Δf	Half power bandwidth
$[\epsilon^*]$	Permittivity tensor
ϵ_r'	Dielectric constant, relative to free space
ϵ_r''	Dielectric loss factor, relative to free space

$\epsilon'' , \epsilon''_{\text{eff}}$	Effective relative loss factor
ϵ^*	Complex permittivity
ϵ_0	Permittivity of free space
ϵ_o	Permittivity of free space
λ	Weight factor ($0 \leq \lambda \leq 1$), representing degree of implicitness
σ	d.c. conductivity
θ_i^{p+1}	Unknown temperature, node i at time $p+1$ ($^{\circ}\text{C}$)
θ_i^p	Known temperature, node i at time p ($^{\circ}\text{C}$)
ρ_l	Density, layer l (kg/m^3)
ω	Circular frequency of electromagnetic radiation, $2\pi f$ (rad/s)
μ	Average dipole moment
μ'_r	Real part of the complex permeability, relative to free space
μ''_r	Imaginary part of the complex permeability, relative to free space
μ_0	Free space permeability

1. Introduction

When using conventional heating methods to heat a coating on a substrate to a temperature above the substrate's softening temperature, heating is difficult or impossible without damaging the substrate. In conventional conductive and convective heating, heat is applied by an external source and then diffuses through the material(s) being heated. For materials with low thermal diffusivities, this process can be very slow. Primary disadvantages of using conventional heating include non-selectivity of heating and continued heating of the materials by diffusion after the heat source has been removed. Microwave heating, on the other hand, has the potential to selectively and volumetrically heat the coating to the desired temperature without damaging the substrate. However, careful design and understanding of the processes involved is necessary for successful application of microwave heating.

In microwave heating, electromagnetic energy is converted to heat volumetrically within the material. The electromagnetic energy is transferred at frequencies between 300 MHz and 30 GHz by waveguides to an applicator which contains the material(s) to be processed. Microwave heating of a material is possible because of the ability of an applied alternating electric

field to polarize bound charges and charged particles within the material(s) and because of the inability of the polarization to stay in phase with the extremely rapid reversals of the electric field (Metaxas and Meredith 1983).

1.1 Microwave Heating Feasibility Study Requirements

In order to evaluate the potential of microwave heating, it is necessary to know the dielectric properties of the materials. The dielectric property which determines a material's ability to propagate and dissipate electromagnetic energy is the complex permittivity. Values of the complex permittivity are unique to each material. They are temperature, frequency, and moisture-content dependent and vary greatly between materials; some materials heat very easily, while others not at all. This results in the potential for selective heating. Selectivity can be a great advantage if the dielectric properties of the two materials are sufficiently different and the desired section(s) can be heated without heating the entire material(s). There are several methods available to determine dielectric properties.

Once the dielectric properties of the materials are known, the feasibility of microwave heating can be evaluated by first determining the heat generation rate required to produce the desired temperature distributions

within the materials by using heat transfer models; second, relating the heat generation results from the heat transfer models to the required electromagnetic field strength during microwave processing; and finally, determining what, if any, equipment is capable of performing the microwave heating.

In order to determine the rate of volumetric heat generation (electromagnetic power dissipation) which would produce the desired temperature distributions within the material(s), heat transfer models of the process are developed. This is complicated because the material properties are often nonuniform and change during processing. As stated previously, the dielectric properties for a material may vary greatly with temperature, frequency, and moisture content. However, by developing appropriate models for the microwave heating, including judicious selection of the model geometry and model assumptions, heat transfer models can be developed which give insight into the effects of initial conditions, heat generation, contact resistance, and convective cooling on the temperature distributions.

The calculated volumetric heat generation rate required to achieve the desired temperature distributions can be used to determine the necessary electric field strength. The theoretical dissipation of electromagnetic power

during microwave heating due to conductive, dielectric, and magnetic losses has been derived using Poynting's theorem. Poynting's theorem is a power balance equation for electromagnetic fields which is derived from Maxwell's equations. This equation leads to an expression for power dissipated during microwave heating. The power dissipation is a function of frequency, the dielectric loss factor of the material being heated, and the electric field strength, and is therefore also coupled with temperature and moisture content. The frequency is equipment dependent, while the electric field strength depends on both the geometry and material being processed, as well as the equipment. Given the dielectric properties of the materials being processed at a given frequency, the estimated heat generation rate, and the expression for theoretical power dissipation, the corresponding electric field strength required is then estimated.

The required electric field strength is then compared to the practical limits of the electric field breakdown strength and the capability of commercially available microwave equipment.

1.2 Microwave Sol-Gel Processing of a Boehmite/ Polypropylene System

As an example of performing a microwave heating feasibility study, microwave sol-gel processing of a temperature-sensitive substrate coated with

a ceramic sol has been investigated. While this specific material system was the impetus for this study, the method developed to determine the feasibility can be applied to many other material combinations. The method consists of a combination of dielectric property determination of the materials, verification of the dielectric properties through experimental heating of the materials, heat transfer modeling of the microwave heating to determine an estimate of the heat generation rates necessary to obtain the desired temperature distribution, and analysis of available microwave heating equipment to determine whether the heat generation rates can be achieved.

In this study, boehmite sol and polypropylene were the specific materials being considered. It has been determined by Kimberly-Clark that sol-gel processing of a boehmite coating while in contact with a temperature-sensitive polypropylene substrate is not possible using conventional heating techniques (Everhart 1994). Sol-gel processing refers to the preparation of ceramic materials by preparation of a sol, gelation of the sol, then subsequent removal of the solvent (Brinker & Scherer 1990). A sol is a colloidal suspension of solid particles in a liquid solvent. Gelation occurs when one molecule reaches macroscopic dimensions so that it extends throughout the solution. For films, the processes of gelation and evaporation dry the sol, resulting in a xerogel film. Xerogels are useful as catalytic substrates and filters due to their high porosity and large surface area. Sintering of a

crystalline xerogel, accomplished by continued heating, leads to dehydration and rearrangement of the crystalline structure, resulting in a series of transitional ceramics and eventually a dense film.

In the case of boehmite, AlOOH , it was desired to dry the boehmite sol or sol-gel, removing all water in the solution, and then to continue heating the resulting xerogel to 250°C , removing chemisorbed (chemically bound) water. Unfortunately, this temperature is above the Vicat softening and melting temperatures of the nonwoven polypropylene substrate, which are 150°C and 171°C , respectively (Brandrup and Immergut 1989). Since sol-gel processing involves the removal of water, both in solution and bound in the chemical structure of the boehmite xerogel, microwave heating was considered as a means of selective heating. Because of its inherent polarity, water is readily heated with microwave energy. Therefore, it seemed possible that the boehmite sol, then the resulting xerogel, could be selectively and volumetrically heated and dried with microwave energy. Desired objectives of the study were to determine the dielectric properties of the boehmite, experimentally show that the boehmite could be successfully heated with microwave energy, and then perform heating of the boehmite coated on the polypropylene substrate.

Since initial experimental attempts to heat the boehmite-coated polypropylene were not successful, the emphasis of the feasibility study shifted to development of heat transfer models of the heating to determine whether the desired heating could be accomplished using other microwave equipment. In this regard, three solutions are presented for the system modeled simply as a substrate of polypropylene fiber coated with boehmite. The primary solution developed is an approximate analytical solution based on the Green's function approach for one-dimensional multilayer slabs. This solution is capable of handling spatially dependent initial temperatures, time and spatially dependent heat generation rates, and finite contact conduction values at the interface between the two materials. The second solution is a cylindrical finite difference solution which allows a constant heat generation rate within each layer, spatially dependent initial temperatures, but no contact conductance between each layer. The third solution is a lumped capacitance solution of the boehmite coating with constant initial temperature and heat generation rate. These solutions were used to determine the theoretical conditions under which successful microwave heating of the boehmite to the desired temperature could be accomplished. This permitted the feasibility of microwave heating for the boehmite/polypropylene system under real conditions to be determined.

1.3 Literature Review

Literature on microwave heating of boehmite or ceramic coatings on polymer substrates was not found. Therefore, the primary focus of the literature review was to develop an understanding of the heat transfer modeling of one dimensional composite media using the Green's function approach.

Use of the Green's function in the solution of partial differential equations in mathematical physics can be found in many sources. Özisik (1993) gives an excellent, well referenced overview of the use of Green's functions in heat transfer problems, including general theory, derivation of necessary equations, and applications to single and multiple layer heat conduction problems with examples in cartesian, cylindrical, and spherical coordinates. It is the primary reference for the equations used in the approximate analytical solution given here. Other related texts include Özisik (1968) and Mikhailov and Özisik (1984). Mathematical proof of the validity of the Green's function method can be found in Carslaw and Jaeger (1959), Morse and Feshback (1953), and Özisik (1968).

Application of the Green's function approach required an understanding of the orthogonal expansion technique. For background on the

orthogonal expansion technique, refer to Özisik (1993), Poulidakos (1994), or other graduate level texts on heat conduction.

There are several key papers and texts on the theory and application of the orthogonal expansion technique and the Green's function approach in the solution of multilayer heat conduction in finite regions.

The first group consists of solutions to the homogeneous solution (without heat generation) of multilayer geometries. Mulholland and Cobble (1972) discuss the use of the Green's function approach in a multilayer slab with perfect contact conductance between the layers. In Lockwood and Mulholland (1973) a similar approach is applied to a hollow cylinder with a circumferentially varying external heat flux. Moore (1967) was the first to find a solution to a multilayer slab which took contact conductance at the interface into account. Mikhailov et al. (1983) discuss the determination of the eigenvalues of a general composite medium with contact conductance, but no heat generation, which can be applied to any coordinate system. The solution of a two layer problem is tested by making both layers the same material.

The second group consists of solutions to the nonhomogeneous heat transfer problem of composite medium with internal heat generation.

Bulavin and Kashcheev (1965) and Portier and Arnas (1975) both present solutions to multilayer cylinder heat transfer problems with heat generation within the layers (but no contact conductance).

1.4 Objectives

The objectives of this study are as follows:

- Develop a methodology to conduct a microwave heating feasibility study for a candidate system consisting of dielectric property determination, development of heat transfer models to determine the heat generation rates necessary to achieve a desired temperature distribution, calculation of the required electric field strength given the dielectric properties and heat generation rates, and examination of whether the microwave heating can be performed with available equipment.
- Apply the methodology to a feasibility study of the microwave sol-gel processing of a boehmite/polypropylene system.

1.5 Overview

Chapter 2 introduces some basic concepts on microwave heating, including discussions on polarization, complex permittivity, and electromagnetic power

dissipation. Chapter 3 discusses details of the experimental work on the boehmite/polypropylene system. It includes details and results of the dielectric property determination for the boehmite, microwave heating experiments on the boehmite, and microwave heating experiments on polypropylene nonwoven coated with boehmite. Chapter 4 provides information on the heat transfer modeling, including determination of the geometry to be modeled and the solutions to the model. Three solutions were developed: an approximate analytical solution, a finite difference solution, and a lumped capacitance solution. Each solution includes a discussion of the governing equations, boundary and initial conditions, and solution assumptions. Chapter 5 presents several test cases which were used to analyze the validity of the solutions developed in Chapter 4. These test cases tested the effects of initial conditions, heat generation, and contact conductance on the approximate analytical solution. In addition, a comparison of the results between the approximate analytical solution and the finite difference solution is provided. Chapter 6 provides details on the theoretical heat generation rate required to heat the boehmite to 250° C, comparison and analysis of the temperature distributions of the different solutions at that heat generation rate, and discussion of the feasibility of achieving that heat generation rate with available microwave processing equipment. Chapter 7 gives conclusions and makes recommendations for future improvements.

While this work included a feasibility study of the microwave heating of a boehmite coating on a temperature sensitive polypropylene substrate, the value of the work extends beyond this specific problem. The principles and methods used here can be used to evaluate other combinations of materials for microwave heating.

With regard to the heat transfer modeling, it is again noted that the two-layer analytical solution developed using Mathematica is capable of handling spatially dependent initial temperatures, time and spatially dependent heat generation rates, and finite contact conduction values at the interface between the two materials. The principles of solving the nonhomogeneous transient heat conduction problem can be extended to more layers or used in cylindrical or spherical coordinates. Heat generation can easily be set to zero to study homogeneous heat transfer. The model could also be used to study other diffusion phenomena. The major limitation to finding the exact analytical solution is the computational power of the computer being used.

2. Theoretical Overview of Microwave Heating

To facilitate understanding of microwave heating, some fundamentals are described in this chapter. A more complete discussion of dielectric loss mechanisms, dielectric properties, and the theoretical aspects of volumetric heating can be found in Metaxas and Meredith (1983). The subjects of polarization, complex permittivity, and volumetric heat generation are presented here as background for why microwave sol-gel processing of the boehmite is being considered and what steps are necessary to determine its feasibility.

2.1 Polarization

Dielectric heating occurs when a material is subjected to an oscillating electric field \vec{E} . The oscillating electric field polarizes the charges within the material, causing them to try to align with the field. This polarization occurs for one of two reasons. For some materials, charge particles within the material are displaced from their equilibrium positions, causing induced dipoles which respond to the electric field. In materials known as polar dielectrics, permanent dipoles (due to asymmetric charge distribution of

unlike charge partners in a molecule) tend to reorientate under the influence of an alternating electric field. These polarized charges and polar molecules are called dipoles. Von Hippel (1954) discusses the primary polarization mechanisms of dielectrics.

The average dipole moment μ of a displaced dipole is given by

$$\mu = qx_i \tag{2-1}$$

where q is the charge and x_i is the distance between the positive and negative charges within the dipole. A polarization field \vec{P} arises which is the sum of all bound dipole moments per unit volume within the dielectric. In free space, the electric charge density due to the externally applied electric field is given by

$$\vec{D}_0 = \epsilon_0 \vec{E} \tag{2-2}$$

where ϵ_0 is the permittivity of free space. A total electric charge flux density vector \vec{D} arises from the sum of the free and bound charge displacements due to the electric field \vec{E}

$$\vec{D} = \vec{D}_0 + \vec{P} \quad (2-3)$$

The total electric charge flux density for a general material is also given as

$$\vec{D} = \epsilon_0 [\epsilon^*] \vec{E} \quad (2-4)$$

where $[\epsilon^*]$ is the permittivity tensor. Using Equations (2-2) through (2-4), the polarization field \vec{P} is defined as

$$\vec{P} = \epsilon_0 ([\epsilon^*] - [1]) \vec{E} \quad (2-5)$$

where $[1]$ is the identity matrix.

2.2 Complex Permittivity

At low frequencies, dipoles have time to reorient with the electric field, which results in energy storage. This storage is described by the dielectric constant ϵ' , otherwise known as real permittivity, and is often described relative to free space. At higher frequencies, the polarization field begins to

lag the electric field, resulting in decreased energy storage. The inability of the polarization to stay in phase with the rapidly reversing electric field causes heating as internal, inelastic, or frictional resistance to dipole motion is converted to kinetic energy. To account for this lag, the permittivity ϵ^* assumes a complex form

$$\epsilon^* = \epsilon' - j\epsilon'' \quad (2-6)$$

where ϵ'' is called the dielectric loss factor, often described relative to free space. The loss factor is the sum of the loss factors for all possible loss mechanisms. At microwave frequencies, the losses are primarily conductive losses and/or dipole or space charge polarization losses. The dielectric loss factor is the key material parameter in microwave heating. When the dielectric properties have been determined (methods are discussed in the next chapter), ϵ'' can then be used to determine the feasibility of microwave heating.

2.3 Volumetric Heat Dissipation

The electromagnetic power dissipated (rate of heat generated) within a material due to conductive, dielectric, and magnetic losses is derived from

Poynting's theorem. Poynting's theorem is essentially a power balance equation derived from Maxwell's equation using electromagnetic fields. The theorem states that the power delivered by an external source is equal to the sum of the power transmitted through the surface, the power dissipated in the volume via magnetic and electric losses, and the reactive energy stored in the volume (Pozar 1990). Poynting's theorem is written as

$$\begin{aligned}
 -\int_s (\vec{E} \times \vec{H}) \cdot d\vec{s} &= \sigma \int_V \vec{E}^2 dV \\
 &+ \omega \int_V (\epsilon_0 \epsilon'_r \vec{E}^2 + \mu_0 \mu'_r \vec{H}^2) dV \\
 &+ j\omega \int_V (\mu_0 \mu'_r \vec{H}^2 - \epsilon_0 \epsilon'_r \vec{E}^2) dV
 \end{aligned}
 \tag{2-7}$$

The surface integral represents the electromagnetic power flow through the surface. The first integral on the right hand side gives the dissipation of electric energy via electronic conduction, where σ is the d.c. conductivity of the volume, V . The second integral represents the electromagnetic energy dissipated by both dielectric and magnetic loss mechanisms, where ϵ_0 is the permittivity of free space and μ_0 is the free space permeability. The subscript r indicates that the property is relative to free space. The last integral represents the electromagnetic energy stored in the volume, where ω is the circular frequency of the electromagnetic radiation. It should be noted here that

magnetic loss mechanisms have been assumed to be negligible in this study and are therefore not discussed further.

Upon use of Maxwell's equations, the average power dissipated (heat generation rate) in an isotropic material in a uniform electric field is found to be

$$P_{av} = \omega \epsilon_0 \epsilon_{eff}'' E_{rms}^2 V \quad (2-8)$$

where ϵ_{eff}'' is the effective relative loss factor accounting for both conductive and dielectric losses, E_{rms} is the root mean squared value of the electric field, and V is the volume of the material. Equation (2-8) highlights the importance of measuring ϵ'' .

Given the importance of knowing the dielectric properties in determining the power dissipation, the focus of the study was to next determine the dielectric properties of the boehmite, and (if these measurements indicated that microwave heating was feasible) to attempt microwave heating of the boehmite/polypropylene system. The next chapter discusses the experimental procedures and results performed to 1) determine

the dielectric properties of the boehmite, 2) heat the boehmite sol-gel, and 3) attempt heating of the boehmite coating on a polypropylene substrate.

3. Experimental Procedures and Results

This chapter details the procedures and results of the experiments on the boehmite/polypropylene system. Experiments were conducted to determine the dielectric properties for the boehmite at various temperatures, to perform microwave heating of dried boehmite sol-gel in a multimode oven, and to attempt microwave heating of a boehmite sol-gel coating on a polypropylene nonwoven in a multimode oven.

3.1 Dielectric Property Determination

The first task in evaluating the feasibility of microwave sol-gel processing of the boehmite sol coating on a polypropylene nonwoven was to determine the dielectric properties of the boehmite. The dielectric properties, most importantly the loss factor, would indicate whether boehmite could be heated using microwave energy. The dielectric properties were found through the cavity perturbation technique using a Hewlett-Packard 8510 Network Analyzer System. Dielectric measurements detailed in this section showed that the boehmite is amenable to microwave heating.

3.1.1 Sample Preparation

Samples for the dielectric testing were prepared from dried boehmite gel provided by Kimberly-Clark. The boehmite was first heated for twenty-four hours at 110° C to drive off moisture. The dried gel was then crushed using a mortar and pestle so that the gel flakes could fit inside KIMAX 51 capillary tubes (1.75 mm inside diameter). Samples were prepared for heating to temperatures between 110° and 250° C. Each capillary tube was weighed, filled with boehmite gel, re-weighed, then heated at its assigned temperature for one hour in a Fisher Scientific Isotemp® Vacuum Oven (Model 282A) and re-weighed again.

3.1.2 Dielectric Testing Using the Cavity Perturbation Technique

3.1.2.1 Background

The cavity perturbation technique is based upon the assumption that low-loss dielectric materials, introduced into an empty resonant cavity, will change the conditions within the cavity only slightly; that these changes in the resonant conditions can be measured; and that the complex permittivity can then be computed, given knowledge of the material geometry (Jackson

1993). A material must meet three criteria in order to use the cavity perturbation technique (Ludman 1994):

- 1) The material must be low-loss and non-ferromagnetic
- 2) Sample sizes must be small relative to the volume of the cavity
- 3) The material must be homogeneous and electrically isotropic

Boehmite meets these requirements once the “wet” sol-gel has been dried.

The cavity perturbation technique determines the complex permittivity of a material at the resonant frequency of a microwave cavity. The resonant cavity in this study was a WR-90 waveguide, which was resonant at 9.4 GHz in a TE_{103} mode. In this mode, the field is transverse electric (TE), with the $TE_{\text{width, height, length}}$ subscripts referring to the number of half wavelengths in the corresponding directions of the waveguide. The electric field of the TE_{103} mode is symmetric in the waveguide with or without a test sample and is maximum at the center of the waveguide. This requires careful placement of the test sample in the center of the provided holes.

When a dielectric material is placed in a resonant cavity, the resonant frequency and cavity Q values decrease slightly. The Q value indicates the bandwidth of the resonant frequency (Ludman 1994). A high Q value indicates a sharp frequency peak resulting from low electrical and magnetic

loss in the cavity. Higher Q values result from the use of highly conductive, polished metals in the resonant cavity. ASTM Standard D2520-86 (1991) recommends Q values of over 2000. Given a high Q, perturbation theory can then be used to accurately compute the complex permittivity from the changes in the resonant frequency and cavity Q factor.

For a more in-depth discussion of perturbation theory and a full derivation of the computations, refer to Jackson (1993) or Altschuler (1963).

3.1.2.2 Equipment

The system used for the dielectric property determination is shown in Figure 3-1. The system is cataloged and described in more detail in Jackson (1993), but an overview is presented here for convenience.

The Hewlett-Packard network analyzer system consists of:

- 1) *Model 8510B Vector Network Analyzer*

A microwave receiver that can process signals from a device to determine the phase and amplitude of the microwaves over a selected frequency band.

2) *Model 8515A S-Parameter Test Unit*

Uses two connector ports (one used in this study) to allow sampling of incident, reflected, and transmitted signals, often referred to as the S-parameters, related to some device-under-test (DUT).

3) *Model 8340A Synthesized Sweeper*

A source of high frequency signals for the system.

4) *Model 9000, Series 300 Computer*

Controls and accesses output from the 8510B to compute the dielectric properties.

5) *Device-Under-Test (DUT)*

The device, in this study's case a WR-90 waveguide, into which the sample is placed. The WR-90 was chosen because of the smaller sample sizes required for dielectric testing (see Table 3-1 for cavity component details). Another resonant cavity, a WR-430, is available but was not used (see Jackson 1993 for details on its use and components). The DUT connects to the 8515A using Gore Model SN S24183 highly flexible coaxial lines with APC-7 connectors.

Error corrections were performed to account for discontinuities, reflections, losses, and imperfections in the coaxial transmission lines. Error calibration was accomplished by measuring known calibration standards, comparing the signal data to theoretical values in an error model, and

mathematically accounting for system imperfections in subsequent computations. The TRL method was used in this study. Details on the TRL Calibration Standard can be found in Jackson (1993) or Ludman (1994).

Four important notes about the calibration: 1) For this study, the Start and Stop Frequencies were 9200 and 9500 MHz, respectively, and the number of points used was 801; 2) Whenever Q was less than 2000, the calibration was redone; 3) When the calibration was saved as calibration set X , calibration set $X+1$ was cleared for use by the `CAVPERT_X` program (to be described below); 4) The calibration was redone if the network analyzer had been turned off or tests had not been conducted in more than a week.

3.1.2.3 Test Procedure

When the TRL calibration was completed, the sample could then be tested. An existing program, "`CAVPERT_X`", was available on disk for use with the WR-90 waveguide ("`CAVPERT`" is used with the WR-430 waveguide). The program is set up for use with samples of cylindrical geometry. For this reason, the inside diameter of the glass tube must be measured and entered. Next, the start and stop frequencies and the number of points used were entered into the program. The iris diameter was checked. The sampling was set to one minute (Menu item 12). Finally, the

temperature measurements were set to “off” (Item 13).

With the menu items correct, the resonant frequency and Q factor of the empty resonant cavity could then be obtained. To remove bias associated with perturbation caused by the KIMAX capillary tubes, an empty tube was placed in the cavity for these measurements. After the “empty” resonant cavity measurements were determined, Calibration Set X+1 in the Network Analyzer was deleted, Correction was set to “ON”, and Calibration Set X was selected. Next the sample was placed in the resonant cavity and the program was continued. The change in the resonant frequency and Q factor were found, then used to compute the complex permittivity per the perturbation method of Jackson (1993) and Altschuler (1963). Based on the previous work of Jackson (1993) and Ludman (1994) using the same system, uncertainty in the dielectric properties, for a sample that completely fills the sample tube, are 1 to 2 % for the dielectric constant and 5 % for the loss factor.

3.1.3 Results

Figure 3-2 shows the measured loss factor of the dried boehmite gel at room temperature for samples prepared by holding them at the specified temperature (abscissa of graph) for one hour in a oven. The dielectric

measurements were made using the perturbation technique at room temperature (the temperature dependence of these measurements may be important but was not measured due to lack of appropriate equipment).

Because the crushed boehmite test samples were not monolithic but packed flakes of gel, there were air spaces in the samples that altered the dielectric properties. This error was corrected by estimating a “fill factor” that was used to adjust the effective diameter, d_{eff} , entered into the CAVPERT_X program. By changing d_{eff} , the effect of the air on the dielectric measurements could be separated, resulting in a more accurate measurement of the dielectric properties of the boehmite. Since the fill factor is difficult to determine accurately and only estimated loss factors were necessary for the feasibility study, the fill factor was estimated as described in the following paragraphs. Estimated upper and lower bounds for the fill factor of 100% and 37.1%, respectively, were used to bound the actual loss factor.

A fill factor of 100 % represents complete packing of the test sample (no air); thus the effective diameter d_{eff} would be the inside diameter d of the KIMAX capillary tube. This gives a lower bound to the loss factor measurements (Figure 3-2). The relationship between d and d_{eff} results through their equivalent volumes:

$$\pi\left(\frac{d}{2}\right)^2 h(\text{Fill Factor}) = \pi\left(\frac{d_{eff}}{2}\right)^2 h \quad (3-1)$$

where h is the height of the resonant cavity. Hence, the effective diameter is related to the fill factor according to

$$d_{eff} = d\sqrt{\text{Fill Factor}} \quad (3-2)$$

To calculate the “fill factor”, the total volume V_{total} of the test sample in the cavity and the neat volume (solid only) were necessary. The total volume was calculated from the height and diameter of the sample in the capillary tube as in Equation (3-1). The neat volume was based on the estimated density and measured mass of the sample material:

$$V_{neat} = \frac{m}{\rho} \quad (3-3)$$

The “fill factor” could then be calculated as

$$\text{Fill Factor} = \frac{V_{neat}}{V_{total}} \quad (3-4)$$

Since the density could not be accurately determined for each heated sample, it was approximated with a constant value of $3,010 \text{ kg/m}^3$, an approximate value based on conversations with Kimberly-Clark. The lower bound on the fill factor corresponded to the sample with the lowest mass after heating (250° C), and was calculated to be 37.1% in this study. This fill factor gave an upper bound for the loss factor as indicated in Figure 3-2.

Allowing for uncertainty in the fill factor, the measured loss factor ϵ'' of the boehmite at 9.4 GHz falls in the range of $0.48 - 1.00$ at 138° C to $0.06 - 0.27$ at 250° C . The decrease in the loss factor over the temperature range of 138° C to 250° C can be attributed to the dehydration of the gel. Materials with loss factors above approximately 0.01 will heat volumetrically in an alternating electric field (EPRI 1987). While published dielectric properties of different materials are difficult to compare because of the various temperatures, frequencies, and moisture contents at which they were obtained, Table 3-2 provides the dielectric properties of several materials for reference (Stern 1994). By comparison, water has a loss factor of 12.0 at 3.0 GHz , and Chaki and Khastgir (1990) report that polypropylene, the material of the nonwoven substrate, has a loss factor of 0.006 at 9.4 GHz . The results of the dielectric material determination indicated that the boehmite could be heated by microwaves.

3.2 Microwave Heating of Boehmite Sol-Gel

With the dielectric property measurements indicating that the microwave heating of boehmite should be possible, the next step in the feasibility study was to confirm it by actually heating the boehmite in a laboratory microwave oven. Tests conducted in a multimode microwave oven and described in this section verified that the boehmite could be successfully heated to the target of 250° C.

3.2.1 Sample Preparation

Kimberly-Clark provided an aqueous Aluminum sol (prepared via hydrolysis of aluminum tris(sec-butoxide)) from which boehmite samples for the microwave heating experiments were prepared. The boehmite sol was heated under vacuum for twenty-four hours at 110° C in the same oven described in Section 3.1.1, producing a dried sol-gel. This procedure was identical to that used by Kimberly-Clark to produce the dried sol-gel used in the dielectric property measurements. The dried sol-gel was then crushed using a mortar and pestle to about the same size used in the dielectric measurements and was placed in a Teflon sample holder, which is shown in Figure 3-3.

3.2.2 Microwave Heating of Boehmite Using a Multimode Microwave Oven

3.2.2.1 Background

A multimode microwave oven was chosen to heat the crushed boehmite sol-gel. A few fundamental characteristics of multimode microwave ovens are given here. For a more detailed description, refer to Chapter 6 of Metaxas and Meredith (1983).

In a microwave oven, microwave radiation is generated by a magnetron and transmitted to an applicator where microwaves are focused into the material being heated. There are several different types of microwave applicators, including traveling wave applicators, single mode resonant cavities, and multimode oven applicators. Traveling wave applicators use transmission lines to propagate the electromagnetic energy continuously, while single mode and multimode cavities use one or more resonant modes, respectively, to store and transfer the microwave energy.

Multimode ovens are designed to produce many resonant modes in the cavity at or near the operating frequency of the magnetron. Since the microwave energy is divided among multiple modes, the electric field

strength of a multimode oven is less than that of a nominally equivalent-power single-mode cavity. Each resonant mode has a distinct resonant frequency and frequency bandwidth. A measure of the bandwidth is the quality factor, Q , defined as

$$Q = \frac{f_r}{\Delta f} \quad (3-5)$$

where f_r is the resonant frequency, and Δf is the half power bandwidth. A high Q indicates a narrow bandwidth, while a low Q indicates a broad bandwidth. Low Q 's are desirable in multimode ovens because the resonant modes are broad and their frequencies overlap, resulting in good coupling with the dielectric material within the cavity for the operating bandwidth of the magnetron (Ludman 1994). Also, the greater number of resonant modes within the cavity results in more uniform heating. The presence of a "lossy" material in the cavity also helps to lower the Q and improves the uniformity of the electric field. Further increases in the uniformity of the electric field can be obtained through the use of a mode stirrer, which continuously perturbs the field distribution.

3.2.2.2 Equipment

The system used in the microwave heating of the boehmite sol-gel is shown in Figure 3-4. The system includes a voltage reducing circuit (Signal Conditioning Box in Figure 3-4) which allows continuous temperature data collection and control of the oven via temperature measurements of the sample from a Luxtron 790 fluoroptic thermometer. It was necessary to design and build this special circuit since oven control and data collection with the available controller can only be done with a type-K thermocouple signal. However, when placed in the microwave oven, a thermocouple tends to concentrate the electric field around its tip, causing both altered and non-uniform heating of the sample, especially if the sample is small. Therefore the signal conditioning circuit was added to convert the output of the less invasive Luxtron probe to emulate a type-K thermocouple. This was possible because the voltage output of a type-K thermocouple as a function of temperature (see National Bureau of Standards 1979) is highly linear over the temperature range 0° to 300° C, deviating by a maximum of 0.4° C from being a linear function of voltage over this temperature range (Figure 3-5). Therefore, it was only necessary to reduce the 0 to 5 V output from the Luxtron to the 0 to 15 mV range of the Type K thermocouple and to calibrate the output at a reference point.

It should be noted that the Luxtron fluoroptic thermometer has an uncalibrated accuracy of $\pm 2.0^{\circ}\text{C}$. Calibrated, the Luxtron has an accuracy of $\pm 0.1^{\circ}\text{C}$ at the calibration point, $\pm 0.5^{\circ}\text{C}$ within $\pm 50^{\circ}\text{C}$ of the calibration point, and $\pm 1.0^{\circ}\text{C}$ within $\pm 100^{\circ}\text{C}$ of the calibration point. When the scale factor is set to $10\text{ mV}/^{\circ}\text{C}$, the temperature range is $\pm 500^{\circ}\text{C}$ and the temperature resolution is 0.24°C .

The multimode microwave oven system consists of the following components (Figure 3-4):

1) *Microwave Materials Technologies (MMT) Model 10-1300 Microwave Furnace*

A multimode microwave oven with a water-cooled magnetron tube capable of producing 1300 W of nominal power at 2450 MHz. The cavity was modified for this study by replacing the glass base of the cavity with a lower loss Teflon base (ϵ'' of 0.003 at 2450 MHz).

2) *Macintosh Quadra 950 with LabVIEW Model 10 Control and DAS Software*

The LabVIEW software allows remote control of the furnace through the Micristar Controller in either a temperature or power mode and provides a data acquisition system (DAS) for various temperature and power outputs from the system.

3) *Micristar Furnace Controller*

A control input/output device capable of both programmed and manual control of the Model 10-1300. Programmed heating can be performed using internal and external programs. The controller can also collect and output power measurements from the Model 10-1300 and temperature measurements from thermocouples.

4) *Luxtron Model 790 Fluoroptic Thermometer*

A fluoroptic thermometer with fiber optic sensors, in this case Luxtron SSC-2 temperature probes with SIWR tips enclosed in low-loss quartz glass sheaths. These sensors perturb the electric field, and therefore the heating, less than thermocouples and also have a faster response time. Output was in the form of a 0 to 5 V linear output which was then reduced to emulate a type-K thermocouple signal.

5) *Signal Conditioning System*

System used to alter the voltage output from the Luxtron to emulate that of a type-K thermocouple. The system consists of a Signal Conditioning Box, which includes a voltage divider tuned with a 10 k Ω variable resistor (potentiometer), and an ice bath, which provides a 0° C reference point for the thermocouple signal output from the box.

6) *Sample and Teflon Sample Holder*

A low dielectric loss, thermally insulating Teflon sample holder (Figure 3-3) was used to hold the sample of crushed boehmite sol-gel.

3.2.2.3 Procedure

Microwave heating tests of the boehmite sol-gel are now described. The first step was to turn on the Luxtron thermometer at least fifteen minutes prior to testing per the manufacturer's instructions. Next, the water cooling system for the magnetron and power switches for the oven and Micristar control unit were turned on. One of the "Scroll" arrow buttons in the lower left of the Micristar control panel was set so that the "PV" light was lit and the top section was set to "% Output" in a similar fashion. The 0° C reference point (at the junction between the two types of wiring) was set in the ice bath. The LabVIEW Model 10 Control and DAS software was started and the "->" button in the top left corner was selected.

Calibration of the thermometry system was accomplished by inserting the Luxtron SSC-2 probe in water heated at 50% power in the cavity. The potentiometer was then adjusted so that the temperature displayed by the

LabVIEW software agreed with the readout from the Luxtron as the water boiled.

With the thermometer calibrated, the boehmite was poured into the Teflon sample holder and placed in the microwave cavity. The Luxtron SSC-2 probe was placed inside a quartz glass sheath and then inserted into the center of the cavity through an access port on the top of the multimode oven and inserted 1/2" into the sample volume.

With the sample ready to be tested, "NEW PROGRAM" was selected on the LabVIEW screen. On the Program Cluster Panel screen, the arrows below "Selected Control Variable" were selected until "Type C" was read. Then for segment 1->2, the following parameters were set: "°C/min" -> "250", "°C" -> "250", "Hold Time (minutes)" -> variable. "Continue" was selected, then "Check Program" on the main panel, to confirm the desired temperature profile from the display. If correct, "Continue" was selected. Next, "Drive Limit (%)" was set to "80" and "DAS (min) Duration" set to the desired time ("60" is the minimum). "Start DAS" was selected, then the button below "Run Auto". The cavity then began heating. The nominal power output (the power generated by the magnetron, not the power absorbed by the sample) increase is indicated on the top display of the Micristar. All

that remained was to monitor the test, then select "Stop DAS" when the test was completed.

3.2.3 Results

The attempts to heat the dried boehmite sol-gel in a multimode microwave oven were successful. As an example, the temperature profile for a boehmite sample heated by microwaves to 260° C, then held at that temperature for one hour, is shown in Figure 3-6. The initial constant slope of the temperature response indicates direct microwave heating, rather than indirect conductive heating from the surroundings. This demonstrates both the ability of microwaves to readily heat boehmite and the successful operation of the modified multimode oven system.

3.3 Microwave Heating of a Boehmite Sol Coating on a Polypropylene Nonwoven

Having successfully heated the boehmite sol-gel in a multimode oven, the last set of experiments were conducted to try to heat a boehmite sol

coating on a polypropylene nonwoven. It was known prior to testing that it would be difficult to succeed for two reasons:

- 1) It was believed that the electric field strength inside the cavity was insufficient to heat the small sample volume to 250° C.
- 2) Surface temperature could not be accurately measured with available equipment (available probes were immersion-type probes only).

3.3.1 Calorimetry Studies of the Electric Field Strength

The average magnitude of the electric field strength incident on the sample in the oven was needed for interpretation of experimental results and accurate numerical modeling. Measurement of the field strength is complicated because the fields are dependent on dielectric loading of the cavity. In other words, they change with sample material, sample holder, and even sample location within the cavity. Field probes would alter the measured electric field, so a calorimetric method was employed. The sample holder and sample location were controlled to be the same as in the heating experiments; only the sample material was changed. Pyrex glass was used since it has dielectric properties which change little with temperature and has better characterized thermophysical properties than boehmite.

Following the method of White (1970), experiments were conducted to estimate the electric field strength E_{rms} using crushed Pyrex glass inside the Teflon sample holder of Figure 3-3. The following analysis describes how the data can give an estimate of field strength. First, consider a control volume around the sample. The change in energy storage per unit volume is for short time steps Δt

$$\frac{\dot{E}_{st}}{V} = \rho c_p \frac{\Delta T}{\Delta t} \quad \text{in} \quad \frac{W}{m^3} \quad (3-6)$$

where ρ and c_p are the density and specific heat, respectively, of the sample.

The heat generation rate per unit volume from microwave sources is

$$\frac{\dot{E}_{gen}}{V} = \omega \epsilon_0 \epsilon_{eff}'' E_{rms}^2 \quad \text{in} \quad \frac{W}{m^3} \quad (3-7)$$

where ϵ_{eff}'' is the effective loss factor of the sample.

If the sample holder is assumed to be perfectly insulated, then

$$\dot{E}_{gen} = \dot{E}_{st} \quad (3-8)$$

Combining Equations (3-6), (3-7), and (3-8), the electric field strength E_{rms} is given by

$$E_{rms} = \frac{\rho c_p}{\omega \epsilon_0 \epsilon''_{eff}} \frac{\Delta T}{\Delta t} \quad (3-9)$$

With material properties known, $\Delta T/\Delta t$ can be measured to give E_{rms} .

Microwave heating of the crushed Pyrex glass was conducted with the multimode oven at 60% power (to avoid damage to the magnetron from reflected power). The value of $\Delta T/\Delta t$ was determined from the measured slope when the conditions of Equation (3-8) were most accurate: when the slope is steepest, since heat loss, storage in the sample holder, and lower field strength would reduce it. From this experiment, it was estimated that the electric field strength was 100,000 V/m and the heat generation rate within the cavity was 1.5×10^8 W/m³.

3.3.2 Sample Preparation

Polypropylene nonwoven provided by Kimberly-Clark was cut into 1" x 1" squares. The nonwoven squares were dipped into the boehmite sol and a roller was used to saturate the nonwoven until there were no dry sections

visible. A square was then transferred to the center of the Teflon floor in the multimode oven. Additional boehmite coating was then applied to the square to ensure saturation.

3.3.3 Equipment

The only aspect of the previously described multimode microwave oven system that was modified for experiments on the coated nonwoven samples was the sample holder. Only the top section of the Teflon sample holder was used. The sample was sandwiched between the Teflon floor and top section as shown in Figure 3-8. The Luxtron temperature probe was inserted through the hole in the sample holder lid until it touched the sample surface.

3.3.4 Results

The attempt to heat a boehmite coated on nonwoven polypropylene was unsuccessful in that the measured temperature did not reach the target of 250° C. Results of the testing are shown in Figure 3-9. Heat losses by conduction and convection overtook the heat generation at approximately 140° C and the maximum temperature reached was approximately 165° C

(Figure 3-9). Two factors restricting heat generation in the sample, which are related by Equation (3-7), have been hypothesized as the cause of not being able to reach 250° C:

- 1) The electric field strength was too low in the multimode cavity
- 2) The coating of boehmite was too small as a percentage of the system (coating and substrate) to provide sufficient heat generation to overcome the losses. Since most of the heat is generated in the lossiest material (the boehmite), the volume of boehmite relative to the total system volume (and heat losses) will determine peak and steady state temperatures.

In summary, not enough heat was generated in the sample to reach desired processing temperatures.

It then became desirable to determine the conditions under which the boehmite/polypropylene system could be successfully heated to 250° C. Heat transfer models developed to answer this question are discussed in the subsequent chapters.

4. Heat Transfer Modeling

Having determined experimentally that the boehmite/polypropylene system did not heat in the available microwave oven, heat transfer modeling was performed to determine the conditions which would be necessary to heat the boehmite to 250° C while it was in contact with the polypropylene. A composite cylinder geometry was selected to approximate the system and then three solutions to the heat transfer model were developed. The solutions were an approximate analytical solution utilizing the Green's function approach for composite slabs, a cylindrical finite difference solution, and a lumped capacitance solution.

4.1 Model Description

The heat transfer models will be based on the microwave heating of a boehmite coating on a temperature-sensitive polypropylene substrate as shown in Figure 4-1. It was decided that a simple model for this geometry consisted of a cylindrical fiber with a coating of uniform thickness. This model represents a worst case scenario (with regard to the dimensional integrity of the nonwoven during processing) in which each fiber in the nonwoven polypropylene is completely coated with boehmite. In fact, the

coating - which is to be as thin as possible - is probably not uniformly distributed. Based on this scenario, a 1-D (one dimensional) heat transfer model consisting of a cylindrical polypropylene fiber of infinite length ($R_1=2.5 \mu\text{m}$) coated with boehmite ($R_2=3.5 \mu\text{m}$) was developed in consultation with the project sponsor (Figure 4-2).

Three solution methods to the model were then considered. The first was an approximate analytical Green's function solution of the governing heat transfer equations using a cartesian coordinate system which approximates the centerline ($r = 0$) condition of the cylindrical model using an insulated boundary condition at $x = 0$ (Figure 4-3). It includes contact conductance at the interface between the two layers ($x = L_1$), time- and space-dependent volumetric heat generation rates $\dot{q}_1'''(x,t)$ and $\dot{q}_2'''(x,t)$, and space-dependent initial temperature distributions $F_1(x)$ and $F_2(x)$. This analytical solution is approximate since the 1-D cylindrical geometry has been simplified to a 1-D cartesian geometry. The second method is a finite difference solution using a cylindrical coordinate system which does not account for contact resistance between the two materials, and has constant volumetric heat generation rates \dot{q}_1''' and \dot{q}_2''' and has uniform initial temperatures F_1 and F_2 (Figure 4-4). The third is an approximate lumped capacitance solution for the boehmite, which assumes that the temperature

response is only time dependent (Figure 4-5), i.e. the spatial variation of temperature is negligible.

4.2 Approximate Analytical Green's Function Solution

4.2.1 Governing Equations

The mathematical formulation of the heat transfer problem shown in Figure 4-3, which is homogeneous in terms of the outer boundary condition, is as follows:

$$\alpha_i \frac{\partial^2 \theta_i}{\partial x^2} + \frac{\alpha_i}{k_i} \dot{q}_i'''(x,t) = \frac{\partial \theta_i}{\partial t}, \quad \text{in } L_{i-1} < x < L_i, \quad t > 0 \quad i = 1,2 \quad (4-1)$$

where

- α_i = Thermal diffusivity, layer i (m^2 / s)
- θ_i = $T_i - T_\infty$ = temperature ($^\circ\text{C}$) in layer i relative to the ambient temperature T_∞ ($^\circ\text{C}$)
- k_i = Thermal conductivity, layer i ($\text{W}/\text{m } ^\circ\text{C}$)
- $\dot{q}_i'''(x,t)$ = Internal heat generation, layer i (W / m^3), a function of position and time
- t = Time (s)
- x = Coordinate location describing distance from the insulated boundary (m)

4.2.2 Spatial Boundary Conditions

The problem is subject to four boundary conditions

$$-k_1 \frac{\partial \theta_1}{\partial x} = 0, \quad x = 0, \quad t > 0 \quad (4-2)$$

$$-k_1 \frac{\partial \theta_1}{\partial x} = h_c (\theta_1 - \theta_2), \quad x = L_1, \quad t > 0 \quad (4-3)$$

$$k_1 \frac{\partial \theta_1}{\partial x} = k_2 \frac{\partial \theta_2}{\partial x}, \quad x = L_1, \quad t > 0 \quad (4-4)$$

$$-k_2 \frac{\partial \theta_2}{\partial x} = h_\infty \theta_2, \quad x = L_2, \quad t > 0 \quad (4-5)$$

where

- h_c = Contact conductance ($W / m^2 \text{ }^\circ\text{C}$) between layers 1 and 2
- h_∞ = Convection heat transfer coefficient ($W / m^2 \text{ }^\circ\text{C}$)
- L_1 = Coordinate of interface between layers 1 and 2 (m)
- L_2 = Coordinate of interface between layers 2 and surroundings (m)

Equation (4-2) is based on an insulated boundary at $x = 0$, Equation (4-3) accounts for contact resistance at the interface between the two materials, Equation (4-4) equates the heat flux between the two layers at the interface, and Equation (4-5) accounts for convection to the surroundings at $x = L_2$.

4.2.3 Initial Conditions

The problem is also subject to the following initial conditions:

$$\theta_i(x, t) = F_i(x), \quad t = 0, \quad i = 1, 2 \quad (4-6)$$

where

$F_i(x)$ = Initial temperature distribution, layer i ($^{\circ}\text{C}$), a function of position

4.2.4 Solution Assumptions

In this solution, it is assumed that the material properties, both heat transfer and dielectric, are assumed to be constant, i.e., independent of temperature and microwave frequency.

4.2.5 Green's Function Solution

The solution to the nonhomogeneous transient heat conduction problem is developed through use of a one-dimensional Composite Green's Function based on the work of Özisik (1993).

4.2.5.1 Eigenvalue Determination

To determine the Green's Function solution, the following eigenvalue problem must be solved (Özisik 1993):

$$\frac{\partial^2 \psi_{in}(x)}{\partial x^2} + \frac{\beta_n^2}{\alpha_i} \psi_{in}(x) = 0, \quad \text{in } L_{i-1} < x < L_i, \quad t > 0 \quad i = 1, 2 \quad (4-7)$$

Subject to

$$\frac{\partial \psi_{1n}}{\partial x}(0) = 0 \quad (4-8)$$

$$-k_1 \frac{\partial \psi_{1n}}{\partial x}(L_1) = h_c (\psi_{1n}(L_1) - \psi_{2n}(L_1)) \quad (4-9)$$

$$k_1 \frac{\partial \psi_{1n}}{\partial x}(L_1) = k_2 \frac{\partial \psi_{2n}}{\partial x}(L_1) \quad (4-10)$$

$$k_2 \frac{\partial \psi_{2n}}{\partial x}(L_2) + h_\infty \psi_{2n}(L_2) = 0 \quad (4-11)$$

where the eigenfunctions are defined as

$$\psi_{1n}(x) = A_{1n} \sin\left(\frac{\beta_n x}{\sqrt{\alpha_1}}\right) + B_{1n} \cos\left(\frac{\beta_n x}{\sqrt{\alpha_1}}\right), \quad 0 < x < L_1 \quad (4-12)$$

$$\psi_{2n}(x) = A_{2n} \sin\left(\frac{\beta_n x}{\sqrt{\alpha_2}}\right) + B_{2n} \cos\left(\frac{\beta_n x}{\sqrt{\alpha_2}}\right), \quad L_1 < x < L_2 \quad (4-13)$$

Applying the eigenfunctions to the boundary conditions, the following equations result

$$A_{1n} = 0, \text{ then arbitrarily set } B_{1n} = 1 \quad (4-14)$$

$$k_1 \frac{\beta_n}{\sqrt{\alpha_1}} \sin\left(\frac{\beta_n L_1}{\sqrt{\alpha_1}}\right) = h_c \left(\cos\left(\frac{\beta_n L_1}{\sqrt{\alpha_1}}\right) - A_{2n} \sin\left(\frac{\beta_n L_1}{\sqrt{\alpha_2}}\right) - B_{2n} \cos\left(\frac{\beta_n L_1}{\sqrt{\alpha_2}}\right) \right) \quad (4-15)$$

$$-k_1 \frac{\beta_n}{\sqrt{\alpha_1}} \sin\left(\frac{\beta_n L_1}{\sqrt{\alpha_1}}\right) = k_2 \frac{\beta_n}{\sqrt{\alpha_2}} \left(A_{2n} \cos\left(\frac{\beta_n L_1}{\sqrt{\alpha_2}}\right) - B_{2n} \sin\left(\frac{\beta_n L_1}{\sqrt{\alpha_2}}\right) \right) \quad (4-16)$$

$$k_2 \frac{\beta_n}{\sqrt{\alpha_2}} \left(A_{2n} \cos\left(\frac{\beta_n L_2}{\sqrt{\alpha_2}}\right) - B_{2n} \sin\left(\frac{\beta_n L_2}{\sqrt{\alpha_2}}\right) \right) + h_\infty \left(A_{2n} \sin\left(\frac{\beta_n L_2}{\sqrt{\alpha_2}}\right) + B_{2n} \cos\left(\frac{\beta_n L_2}{\sqrt{\alpha_2}}\right) \right) = 0 \quad (4-17)$$

Next define

$$a_1 = \frac{\beta_n}{\sqrt{\alpha_1}} \quad a_2 = \frac{\beta_n}{\sqrt{\alpha_2}} \quad \gamma = \frac{\beta_n L_1}{\sqrt{\alpha_1}} \quad \eta = \frac{\beta_n L_2}{\sqrt{\alpha_2}}$$

$$K = \frac{k_1}{k_2} \quad \alpha = \frac{\sqrt{\alpha_2}}{\sqrt{\alpha_1}} \quad h_1 = \frac{k_1}{h_c} \quad h_2 = \frac{k_2}{h_\infty} \quad \ell = \frac{L_1}{L_2}$$

where the only unknowns are the eigenvalues β_n .

Putting Equations (4-15), (4-16), and (4-17) in matrix form gives

$$\begin{bmatrix} h_1 a_1 \sin \gamma - \cos \gamma & \sin \ell \eta & \cos \ell \eta \\ K \alpha \sin \gamma & \cos \ell \eta & -\sin \ell \eta \\ 0 & h_2 a_2 \cos \eta + \sin \eta & -h_2 a_2 \sin \eta + \cos \eta \end{bmatrix} \begin{bmatrix} 1 \\ A_{2n} \\ B_{2n} \end{bmatrix} = \begin{bmatrix} 0 \\ 0 \\ 0 \end{bmatrix} \quad (4-18)$$

Solving rows 2 and 3 of Equation (4-18) for A_{2n} and B_{2n}

$$A_{2n} = \sin \ell\eta(\cos \gamma - h_1 a_1 \sin \gamma) - K\alpha \sin \gamma \cos \ell\eta \quad (4-19)$$

$$B_{2n} = \cos \ell\eta(\cos \gamma - h_1 a_1 \sin \gamma) + K\alpha \sin \gamma \sin \ell\eta \quad (4-20)$$

The equation for determination of the eigenvalues β_n results from the matrix form of the boundary condition equations above. From that equation it is seen that for the equations to be valid

$$\det \begin{vmatrix} h_1 a_1 \sin \gamma - \cos \gamma & \sin \ell\eta & \cos \ell\eta \\ K\alpha \sin \gamma & \cos \ell\eta & -\sin \ell\eta \\ 0 & h_2 a_2 \cos \eta + \sin \eta & -h_2 a_2 \sin \eta + \cos \eta \end{vmatrix} = 0 \quad (4-21)$$

The determinant and its roots (β_n 's) were found using Mathematica™.

4.2.5.2 Transient Temperature Distribution Determination

Once the eigenvalues β_n 's are known, the eigenfunctions $\psi_{1n}(x)$ and $\psi_{2n}(x)$ are calculated. The norm N_n is then computed

$$N_n = \sum_{j=1}^2 \frac{k_j}{\alpha_j} \int_{L_{j-1}}^{L_j} \psi_{jn}^2(x') dx' \quad (4-22)$$

Having now found $\psi_{1n}(x)$, $\psi_{2n}(x)$, and N_n , the composite medium Green's functions can be calculated:

$$G_{ij}(x, t | x', \tau) = \sum_{n=1}^{\infty} e^{-\beta_n^2(t-\tau)} \frac{1}{N_n} \frac{k_j}{\alpha_j} \psi_{in}(x) \psi_{jn}(x'), \quad j=1,2 \quad (4-23)$$

Thus with the Green's functions known, the transient temperature distribution is found to be

$$\begin{aligned} T_i(x, t) = & \int_{x'=0}^{L_1} [G_{i1}(x, t | x', \tau)]_{\tau=0} F_1(x') dx' \\ & + \int_{x'=L_1}^{L_2} [G_{i2}(x, t | x', \tau)]_{\tau=0} F_2(x') dx' \\ & + \int_{\tau=0}^t \int_{x'=0}^{L_1} G_{i1}(x, t | x', \tau) \frac{\alpha_1}{k_1} \dot{q}_1''(x', \tau) dx' d\tau \\ & + \int_{\tau=0}^t \int_{x'=L_1}^{L_2} G_{i2}(x, t | x', \tau) \frac{\alpha_2}{k_2} \dot{q}_2''(x', \tau) dx' d\tau \\ & + T_{\infty} \end{aligned} \quad (4-24)$$

Mathematica has been used to perform the calculations for the approximate analytical solution (see Appendix A). The validation and results of the model are presented in Chapters 5 and 6.

4.3 Finite Difference Solution

4.3.1 Governing Equations

The mathematical formulation of the heat transfer problem using the geometry in Figure 4-4 is as follows:

$$\alpha_i \frac{1}{r} \frac{\partial}{\partial r} \left(r \frac{\partial \theta_i}{\partial r} \right) + \frac{\alpha_i}{k_i} \dot{q}_i'''(r,t) = \frac{\partial \theta_i}{\partial t}, \quad \text{in } R_{i-1} < r < R_i, \quad t > 0 \quad i = 1, 2 \quad (4-25)$$

where

- α_i = Thermal diffusivity, layer i (m^2 / s)
 θ_i = $T_i - T_\infty$ = temperature ($^\circ\text{C}$) in layer i relative to the ambient temperature T_∞
 k_i = Thermal conductivity, layer i ($\text{W}/\text{m } ^\circ\text{C}$)
 $\dot{q}_i'''(r, t)$ = Internal heat generation rate, layer i (W / m^3), a function of position and time
 t = Time (s)
 r = Radial coordinate describing distance from centerline (m)

4.3.2 Spatial Boundary Conditions

The problem is subject to several boundary conditions:

$$-k_1 \frac{\partial \theta_1}{\partial r} = 0, \quad r = 0, \quad t > 0 \quad (4-26)$$

$$\theta_1 = \theta_2, \quad r = R_1, \quad t > 0 \quad (4-27)$$

$$k_1 \frac{\partial \theta_1}{\partial r} = k_2 \frac{\partial \theta_2}{\partial r}, \quad r = R_1, \quad t > 0 \quad (4-28)$$

$$-k_2 \frac{\partial \theta_2}{\partial r} = h\theta_2, \quad r = R_2, \quad t > 0 \quad (4-29)$$

This differs from the previous analytical solution in that the effect of contact conductance at the interface is not accounted for, and thus the temperatures within each layer at the interface are equal.

4.3.3 Initial Conditions

The problem is also subject to the following initial conditions:

$$T_i(r, t) = F_i(r), \quad t = 0, \quad i = 1, 2 \quad (4-30)$$

where

$F_i(r)$ = Initial temperature distribution, layer i ($^{\circ}\text{C}$), a function of position

4.3.4 Solution Assumptions

As in the previous solution, it is assumed that the material properties, both heat transfer and dielectric, are assumed to be constant, i.e. independent of temperature and microwave frequency.

4.3.5 Finite Difference Solution Nodal Equations

For the finite difference model, $0 \leq r \leq R_2$ is divided into a total of N nodes (Figure 4-6), M nodes in $0 \leq r \leq R_1$ and $N-M+1$ nodes in $R_1 \leq r \leq R_2$, such that the spacing of the nodes in the respective regions Δr_1 and Δr_2 is

$$\Delta r_1 = \frac{R_1}{M-1} \text{ and } \Delta r_2 = \frac{R_2 - R_1}{N-M}$$

The mixed, or combined, method is used in determining the nodal equations from an energy balance around each node. A FORTRAN program was written to solve for the transient nodal temperatures $T_i(r, t)$ (see Appendix B).

4.3.5.1 Center Node - Node 1

Based on an energy balance, the following nodal equation for the temperatures at the center node is obtained:

$$(1 + 4f_1\lambda)\theta_1^{p+1} - 4f_1\lambda\theta_2^{p+1} = (1 - 4f_1(1-\lambda))\theta_1^p + 4f_1(1-\lambda)\theta_2^p + \frac{\dot{q}_1'''}{k_1}\alpha_1\Delta t \quad (4-31)$$

where in general

$$f_i = \frac{\alpha_i\Delta t}{\Delta r_i^2}$$

and

- λ = Weight factor ($0 \leq \lambda \leq 1$), representing degree of implicitness
- θ_i^{p+1} = Unknown temperature ($^{\circ}\text{C}$), node i at time $p+1$
- θ_i^p = Known temperature ($^{\circ}\text{C}$), node i at time p

$\dot{q}_1''' =$ Internal heat generation rate (W / m^3), in layer 1

4.3.5.2 Internal Node i, Layer 1 (polypropylene)

Based on an energy balance, the following nodal equation for the temperatures in the interior of Layer 1 is obtained:

$$\begin{aligned}
 -f_1 g_{m1} \lambda \theta_{i-1}^{p+1} + (1 + 2f_1 \lambda) \theta_i^{p+1} - f_1 g_{p1} \lambda \theta_{i+1}^{p+1} = \\
 f_1 g_{m1} (1 - \lambda) \theta_{i-1}^p + (1 - 2f_1 (1 - \lambda)) \theta_i^p + f_1 g_{p1} (1 - \lambda) \theta_{i+1}^p + \frac{\dot{q}_1'''}{k_1} \alpha_1 \Delta t
 \end{aligned} \tag{4-32}$$

where

$$g_{m1} = \left(1 - \frac{\Delta r_1}{2R_1} \right) \quad \text{and} \quad g_{p1} = \left(1 + \frac{\Delta r_1}{2R_1} \right)$$

4.3.5.3 Interface Node M

Based on an energy balance, the following nodal equation for the temperatures at the interface between Layers 1 and 2 is obtained:

$$\begin{aligned}
 -Fo_1 g_{m1} \lambda \theta_{m-1}^{p+1} + \left(1 + \lambda (Fo_1 g_{m1} + Fo_2 g_{p1}) \right) \theta_m^{p+1} - Fo_2 g_{p1} \lambda \theta_{m+1}^{p+1} = \\
 Fo_1 g_{m1} (1 - \lambda) \theta_{m-1}^p + \left(1 - (Fo_1 g_{m1} + Fo_2 g_{p1}) (1 - \lambda) \right) \theta_m^p + \\
 Fo_2 g_{p1} (1 - \lambda) \theta_{m+1}^p + \frac{\dot{q}_1'''}{k_1} \frac{Fo_1}{2\Delta r_1^2} + \frac{\dot{q}_2'''}{k_2} \frac{Fo_2}{2\Delta r_2^2}
 \end{aligned} \tag{4-33}$$

where

$$Fo_1 = \frac{2k_1 \Delta t}{\Delta r_1 (\rho_1 c_{p1} \Delta r_1 + \rho_2 c_{p2} \Delta r_2)}$$

and

$$Fo_2 = \frac{2k_2 \Delta t}{\Delta r_2 (\rho_1 c_{p1} \Delta r_1 + \rho_2 c_{p2} \Delta r_2)}$$

4.3.5.4 Internal Node I, Layer 2 (boehmite)

Based on an energy balance, the following nodal equation for the temperatures in the interior of Layer 2 is obtained:

$$-f_2 g_{m2} \lambda \theta_{i-1}^{p+1} + (1 + 2f_2 \lambda) \theta_i^{p+1} - f_2 g_{p2} \lambda \theta_{i+1}^{p+1} = \quad (4-34)$$

$$f_2 g_{m2} (1 - \lambda) \theta_{i-1}^p + (1 - 2f_2 (1 - \lambda)) \theta_i^p + f_2 g_{p2} (1 - \lambda) \theta_{i+1}^p + \frac{\dot{q}_2'''}{k_2} \alpha_2 \Delta t$$

where

$$g_{m2} = \left(1 - \frac{\Delta r_2}{2R_2}\right) \quad \text{and} \quad g_{p2} = \left(1 + \frac{\Delta r_2}{2R_2}\right)$$

4.3.5.5 Convection Surface, Node N

Based on an energy balance, the following nodal equation for the temperatures at the convection boundary surface is obtained:

$$\begin{aligned}
-f_2 g_{m2} \lambda \theta_{N-1}^{p+1} + (1 + 2f_2 \lambda (g_{m2} + Bi)) \theta_N^{p+1} = & \quad (4-35) \\
2f_2 g_{m2} (1 - \lambda) \theta_{N-1}^p + (1 - 2f_2 (1 - \lambda) (g_{m2} + Bi)) \theta_N^p + \frac{\dot{q}_2'''}{k_2} \alpha_2 \Delta t
\end{aligned}$$

where

$$Bi = \frac{h_\infty \Delta r_2}{k_2},$$

is the numerical Biot number for layer 2. Results of this model are presented in Chapters 5 and 6.

4.4 Approximate Lumped Capacitance Method

To determine whether the lumped capacitance method is valid, the Biot number must first be calculated to insure that the following condition is met:

$$Bi = \frac{h_\infty L_c}{k} \leq 0.1 \quad (4-36)$$

where L_c is the characteristic length V/A_s , V is the volume of the region per unit cylinder length, defined as

$$V' = \pi(R_2^2 - R_1^2) \quad (4-37)$$

and A'_s is the surface area per unit cylinder length, defined as

$$A'_s = 2\pi R_2 \quad (4-38)$$

When this condition is met, the spatial temperature distribution within the region is relatively uniform. Therefore the temperature can be approximated as a function of time only.

Since the lumped capacitance method does not include spatial variation, only a homogeneous material with one boundary may be modeled (Figure 4-5). Therefore, as an approximation consider only the effects of heat generation within the boehmite and convection at its interface with the surroundings. This assumes that the heat transfer from the boehmite (Material 2) to the polypropylene (Material 1) is much smaller than the heat transfer to the convective fluid, i.e. the interface boundary is assumed to be insulated. Taking an energy balance on the boehmite layer

$$\dot{E}_{in} - \dot{E}_{out} = \dot{E}_{st} \quad (4-39)$$

or per unit cylinder length

$$\dot{q}_2 V' - h A'_s \theta = \rho V' c_p \frac{d\theta}{dt} \quad (4-40)$$

The equation is then rewritten in terms of $\theta(t) = T - T_\infty$ resulting in the following first order, linear differential equation to be solved:

$$\frac{d\theta}{dt} + \frac{h_\infty}{\rho L_c c_p} \theta = \frac{\dot{q}_2'''}{\rho L_c c_p} \quad (4-41)$$

Next apply the following initial condition:

$$\theta(t = 0) = \theta_0 = T_0 - T_\infty \quad (4-42)$$

The resulting equation for $T(t) = \theta(t) + T_\infty$ determined using Mathematica™, is

$$T(t) = \left(T_0 - T_\infty - \frac{L_c \dot{q}_2'''}{h_\infty} \right) e^{-\left(\frac{h_\infty t}{\rho L_c c_p} \right)} + \frac{L_c \dot{q}_2'''}{h_\infty} + T_\infty \quad (4-43)$$

Having developed the three solutions to the chosen heat transfer model, the next step is to verify the solutions by applying test cases. This is the subject of the next chapter.

5. Validation of the Approximate Analytical Solution

Having developed the heat transfer models in the previous chapter, the approximate analytical heat transfer model is now validated by testing the effects of the initial condition, heat generation, and contact conductance terms.

The effects of the initial conditions and the application of heat generation are separately checked by applying the approximate analytical model to cases for which an analytical solution is previously known. In these example cases, the two-layer analytical model is used in the solution of a one material heat transfer problem by making the material properties the same within each of the layers and setting the contact conductance between the two layers to infinity (i.e., contact resistance is zero). To further examine model validity, steady state temperatures are evaluated to determine under what conditions the analytical model is a good approximation of the cylindrical geometry.

Finally, to check the effect of contact conductance on the model, a third example case is presented. It is similar to the second example, except that heat generation is applied only to the outer layer and finite contact conductances

are applied. The effect of applying finite contact conductance is then studied, without benefit of a previously found analytical solution.

5.1 Initial Condition Analysis

Test Case 1: A long sheet (plane wall) of thickness $2L$, initially at temperature T_o , is suddenly immersed in a cold liquid bath of temperature T_∞ (from Poulidakos 1994, Example 5.1, p 116-121).

This system is illustrated in Figure 5-1. The governing equation for the one-dimensional homogeneous transient heat transfer problem is

$$\frac{\partial^2 \theta}{\partial x^2} = \frac{1}{\alpha} \frac{\partial \theta}{\partial t} \quad \text{in } 0 < x < L \quad (5-1)$$

where $\theta = T - T_\infty$ subject to the conditions

$$\frac{\partial \theta}{\partial x} = 0 \quad \text{at } x = 0 \quad (5-2)$$

$$-k \frac{\partial \theta}{\partial x} = h_\infty \theta \quad \text{at } x = L \quad (5-3)$$

$$\theta = \theta_o \quad \text{at } t = 0 \quad (5-4)$$

Using the method of separation of variables, the expression for the temperature is

$$T(x,t) = T_{\infty} + (T_o - T_{\infty}) \sum_{n=1}^{\infty} \frac{\sin(\beta_n R)}{\frac{\beta_n R}{2} + \frac{\sin(2\beta_n R)}{4}} \cos(\beta_n x) e^{-\alpha \beta_n^2 t} \quad (5-5)$$

This solution was compared to the approximate analytical solution, which was modified to reflect the conditions of Equations (5-1) to (5-4). Each series solution was based on an n of five. Table 5-1 lists the dimensional values used to compute and compare the solutions. The properties used are those of boehmite, but the system dimension (length) is orders of magnitude larger than the system of interest to Kimberly-Clark (the subject of Chapter 6).

The greatest error in the analytical solution occurs at $t = 0$ (Figure 5-2). While the temperature should be uniform at $T_o = 125^{\circ} \text{C}$, there is temperature error in both the analytical and Poulidakos solutions. The error in the analytical solution is less than 1.5°C in $0 \leq x \leq 0.95 L$, but then increases to 5.3°C at $x = L$. This error is a result of limiting the number of terms used to compute the composite Green's function; changing the number of terms from two to five reduced the discrepancy by 5°C . Further increases in the number of terms evaluated would further decrease the error. The same data are plotted with an expanded scale in Figure 5-3 ($t = 0$) to show the relative

significance of the discrepancy with five terms. Using five terms appears to be sufficient to give the required accuracy for all times.

Figure 5-3 shows the comparison of the transient spatial temperature distribution of the two models at different times. The composite Green's function solution is indistinguishable from the accepted solution by Poulidakos within ten seconds even though the temperature is still very close to the initial distribution. This provides confidence that the composite Green's function solution is valid for initial condition problems. More than five terms of the solution would be required only if more accurate results were needed.

5.2 Heat Generation Analysis

Test Case 2: A long cylinder of radius R is initially at temperature T_0 . For time $t > 0$ heat is generated volumetrically within the cylinder at a constant rate \dot{q}''' and heat is dissipated by convection with an ambient temperature T_∞ at $r=R$ (from Özisik 1968, p 149-151).

This system is shown in Figure 5-4. The governing equation for the nonhomogeneous transient heat conduction problem is

$$\frac{\partial^2 \theta}{\partial r^2} + \frac{1}{r} \frac{\partial \theta}{\partial r} + \frac{\dot{q}'''(r, t)}{k} = \frac{1}{\alpha} \frac{\partial \theta}{\partial t} \quad \text{in } 0 < r < R \quad (5-6)$$

where $\theta = T - T_\infty$ subject to the conditions

$$k \frac{\partial \theta}{\partial r} + h_\infty \theta = f_2(t) \quad \text{at } r = R, \quad t > 0 \quad (5-7)$$

$$\theta = F(r) \quad \text{in } 0 \leq r \leq R, \quad t = 0 \quad (5-8)$$

Using the integral transform technique, Özisik found the solution to be

$$T(r, t) = T_\infty + \sum_{n=1}^{\infty} e^{-\alpha \beta_n^2 t} \cdot K_0(\beta_n, r) \cdot \left[\bar{F}(\beta_n) + \int_{r'=0}^t e^{\alpha \beta_n^2 t'} \cdot A(\beta_n, t') \cdot dt' \right] \quad (5-9)$$

where

$$A(\beta_n, t') = \frac{\alpha}{k} g(\beta_n, t') + \alpha \cdot R \cdot \left. \frac{K_0(\beta_n, r)}{k} \right|_{r=R} \cdot f_2(t') \quad (5-10)$$

$$\bar{g}(\beta_n, t') = \int_{r'=0}^R r' \cdot K_0(\beta_n, r') \cdot g(r', t') \cdot dr' \quad (5-11)$$

$$\bar{F}(\beta_n) = \int_{r'=0}^R r' \cdot K_0(\beta_n, r') \cdot F(r') \cdot dr' \quad (5-12)$$

$$K_0(\beta_n, r) = \frac{\sqrt{2}}{R} \frac{\beta_n}{[H^2 + \beta_n^2]^{1/2}} \cdot \frac{J_0(\beta_n r)}{J_0(\beta_n R)} \quad (5-13)$$

and the eigenvalues β_n are the positive roots of the transcendental equation

$$\frac{\beta J_1(\beta R)}{J_0(\beta R)} = \frac{h_\infty}{k} \quad (5-14)$$

and $J_0(\beta r)$ is the Bessel function of the first kind of order 0.

Since the analytic solution is cartesian (plane wall), an appropriate choice for L was made to approximately model the cylindrical problem of Test Case 2. The global steady state energy generation was equated by forcing the heat fluxes at the convection boundary to be equal. Setting the heat flux (and hence the temperature) at the boundary to be the same for both geometries gives

$$L = R/2 \tag{5-15}$$

The same relationship results from using the conventional characteristic length (volume/surface area) for both geometries. Therefore, the “equivalent” cartesian (plane wall) model of the cylindrical geometry has a thickness of only one-half the cylinder radius. The implications of this transformation are discussed further in Section 5.2.2.

The analysis of this test case is divided into two sections: comparison of the approximate analytical solution with a cartesian steady state solution, and comparison of the approximate analytical solution with the known cylindrical solution from Özisik.

5.2.1 Approximate Analytical Model and Cartesian Steady State Solution Comparison

The plane wall geometry and conditions in Test Case 2 are equivalent to those of the plane wall problem discussed in Section 3.5.1, p. 108-111, of Incropera and Dewitt 1990. The steady state solution to that problem,

$$T(x) = \frac{\dot{q}L^2}{2k} \left(1 - \left(\frac{x}{L} \right)^2 \right) + T_\infty + \frac{\dot{q}L}{h} \quad (5-16)$$

has been used for comparison. Figure 5-5 shows the difference between this solution and the analytical Green's function solution using the dimensional values listed in Table 5-1 and $\dot{q}''' = 275,000 \text{ W/m}^3$. The maximum temperature difference is 1.7°C at $x = 0$, which is considered sufficiently close. This provides further evidence of the validity of the model in solving problems with internal heat generation in the cartesian coordinate system.

5.2.2 Approximate Analytical Solution and Cylindrical Solution Comparison

Comparison of results from the analytical solution with the Özisik solution revealed considerable differences between the two solutions (Figure 5-6 through 5-8). The models are not expected to agree completely because one is cartesian and the other cylindrical. At the convective boundary (Figure

5-8), the results are close, as expected, since the spatial dimensions of the models were selected to equate steady state heat fluxes for both solutions at this boundary ($x/L = r/R = 1$). The maximum temperature difference between the solutions occurs in the center at steady state and is approximately 164°C (Figure 5-6) for Test Case 2. The temperature is higher for the cylindrical solution than for the cartesian solution for any $x/L = r/R$ except $x/L = 1$. This is consistent with the use of $L = R/2$ to relate the plane wall model to the cylindrical geometry (Section 5.2). The convective surface temperatures were forced to be the same (at steady state), but the plane wall is half as thick as the radius of the cylinder and hence does not reach the internal temperatures of the cylinder.

Thus the question arises, under what conditions is the approximate analytical solution valid in estimating the temperature distribution for the cylindrical case of interest (i.e., when is the geometric simplification acceptable). This is a complicated issue, since it is affected by the heat generation rates, material properties, and thicknesses of each material, as well as the time period of interest and the convection heat transfer coefficient. An upper bound on the maximum temperature difference (i.e., the greatest error in the analytical cartesian approximation) can be determined from the maximum difference (worst case) at steady state at the center ($x, r = 0$). To develop the upper bound, the two-layer, steady state, plane wall heat transfer

problem with heat generation and contact resistance and its cylindrical counterpart are then solved and related. The resulting spatially dependent, steady state temperature distributions within each layer are in cartesian coordinates,

$$T_1(x) = T_\infty + \frac{\dot{q}_1}{2k_1}(L_1^2 - x^2) + \frac{\dot{q}_2}{2k_2}(L_2^2 - L_1^2) + \frac{L_1}{k_2}(\dot{q}_2 - \dot{q}_1)(L_1 - L_2) + \frac{L_1\dot{q}_1 + (L_2 - L_1)\dot{q}_2}{h_\infty} + \frac{L_1\dot{q}_1}{h_c} \quad (5-17)$$

$$T_2(x) = T_\infty + \frac{\dot{q}_2}{2k_2}(L_2^2 - x^2) + \frac{L_1}{k_2}(\dot{q}_2 - \dot{q}_1)(x - L_1) + \frac{L_1\dot{q}_1 + (L_2 - L_1)\dot{q}_2}{h_\infty} \quad (5-18)$$

and in cylindrical coordinates, substituting $R_1 = 2L_1$ and $R_2 = 2L_2$,

$$T_1(r) = T_\infty + \frac{\dot{q}_1}{4k_1}(L_1^2 - r^2) + \frac{\dot{q}_2}{k_2}(L_2^2 - L_1^2) + \frac{2L_1^2}{k_2}(\dot{q}_2 - \dot{q}_1)(\ln(2L_1) - \ln(2L_2)) + \frac{L_1^2\dot{q}_1 + (L_2^2 - L_1^2)\dot{q}_2}{h_\infty L_2} + \frac{L_1\dot{q}_1}{h_c} \quad (5-19)$$

$$T_2(r) = T_\infty + \frac{\dot{q}_2}{4k_2}(4L_2^2 - r^2) + \frac{2L_1^2}{k_2}(\dot{q}_2 - \dot{q}_1)(\ln r - \ln(2L_2)) + \frac{L_1^2\dot{q}_1 + (L_2^2 - L_1^2)\dot{q}_2}{h_\infty L_2} \quad (5-20)$$

Given the material properties and geometry, the cartesian and cylindrical solutions can then be computed and compared at the center to determine the

upper bound of the maximum temperature difference between the two models for any material combination.

To analyze Test Case 2 at the center, Equations (5-17) through (5-20) are modified by setting the material properties and heat generation rates the same within each layer, L_1 equal to zero, and h_c equal to Infinity. The resulting equations are the same as those in Section 3.5 of Incropera & Dewitt, 1990:

$$T(x = 0) = \frac{\dot{q}L^2}{2k} + \frac{\dot{q}L}{h_\infty} + T_\infty \quad (5-21)$$

$$T(r = 0) = \frac{\dot{q}L^2}{k} + \frac{\dot{q}L}{h_\infty} + T_\infty \quad (5-22)$$

Two plots have been generated based on the material properties of the test case listed in Table 5-1 to compare the difference between Equations (5-21) and (5-22). Figure 5-9 shows the increase in the difference at steady state (maximum difference) between the two models as a function of material thickness L up to the thickness of Test Case 2 ($L = 5$ cm) for various heat generation rates (W/m^3). The difference is small for smaller thicknesses and heat generation rates but increases rapidly as the heat generation rate increases (Figure 5-6 showed the transient difference in maximum temperature between the two models at $L = 5$ cm with a heat generation rate

of $275,000 \text{ W/m}^3$). Figure 5-10 shows the temperature differences for very small thicknesses (on the order of microns) in the range of the research model (Chapters 4 and 6) at various heat generation rates. For the research model thickness $L_2 = 2.5 \times 10^{-6} \text{ m}$, thermal conductivity $k = 2.1 \text{ W/m}\cdot\text{K}$ and heat generation rate,

$$\dot{q}''' = 1 \times 10^x \quad (5-23)$$

in W/m^3 , the relationship for the maximum predicted temperature difference from Equations (5-21) and (5-22) is

$$\Delta T_{\max} = 6.44 \times 10^{x-12} \text{ }^\circ\text{C} \quad (5-24)$$

Therefore, for the research model system with the heat generation rate required to heat the boehmite to a steady state temperature of $250 \text{ }^\circ\text{C}$ in the multimode oven being approximately $8.1 \times 10^8 \text{ W/m}^3$ ($x \approx 9$), the predicted maximum temperature difference is of the order of $10^{-3} \text{ }^\circ\text{C}$. This indicates that the cartesian analytical solution is a valid approximation to the cylindrical problem when the system dimensions are small (order of microns).

5.3 Contact Conductance Analysis

Test Case 3: A long sheet (plane wall) of thickness $2L$, insulated at the surface $x = 0$, is initially at temperature T_0 . The sheet is composed of two layers of the same material, but contact resistance exists between the two layers. For time $t > 0$, heat is generated volumetrically within the region $L \leq x \leq 2L$ at a constant rate \dot{q}''' and heat is dissipated by convection with an ambient temperature T_∞ at $x = 2L$.

The geometry of this test case is identical to that of the approximate analytical model in Chapter 4. During the literature search no published solutions were found which combine internal heat generation and contact resistance. To check the validity of the contact conductance term, the heat flux at the contact surface was checked to ensure that the condition

$$-k_1 \frac{\partial T_1}{\partial x} = h_c (T_1(L) - T_2(L)) \quad (5-25)$$

was met at the interface. This condition was verified for several values of h_c .

Having determined that Equation (5-25) was satisfied, the effect of the contact conductance at the interface h_c on the temperature difference at the

interface was then studied for Test Case 3. This temperature difference is key to the proposed application of processing a layer of material at an elevated temperature, while it is contact with another temperature-sensitive material. Figure 5-11 shows the increase in the temperature difference between the two layers as the contact conductance at the interface decreases (contact resistance increases). Figure 5-12 shows the maximum temperature difference (at any time) between the layers as a function of the contact resistance at the interface, $1/h_c$. This shows, as expected, that the contact resistance must be high in order to obtain appreciable temperature differences. For this example, the contact conductance coefficient must be of lower magnitude than a typical forced convection heat transfer coefficient (less than $100 \text{ W / m}^2 \cdot \text{K}$) to achieve an interface temperature difference greater than 20°C . Also of interest is the relationship between the time to reach the maximum ΔT at the interface and the contact conductance, shown in Figure 5-13. As the contact conductance decreases, the time required to reach the maximum ΔT increases. Thus, for a given material combination and heat generation rate, a higher desired ΔT at the interface means that a longer processing time will be required. It must be remembered, however, that the magnitudes of the temperatures on both sides of the interface are also increasing with time. Therefore the achievable ΔT may be limited by the temperature-sensitive material. To decrease the processing time, the heat generation rate must be increased.

In this chapter, the effects of initial conditions, internal heat generation, and contact resistance have been tested for the approximate analytical solution. With sufficient confidence in this solution achieved, the next chapter will discuss the results of applying the heat transfer solutions to sol-gel processing of the boehmite/polypropylene system.

6. Results of the Heat Transfer Modeling

The heat transfer models were used to determine the conditions under which the boehmite coating could be heated to 250° C without degrading the polypropylene substrate significantly. The models were used to determine the temperature distribution within both layers when a heat generation rate \dot{q}_2''' was applied to the boehmite coating so that the temperature of the boehmite at the boehmite/polypropylene interface would reach 250°C, while keeping the majority of the polypropylene under 150° C. Although a heat generation rate \dot{q}_2''' was found which produced favorable temperature distributions, it was beyond the practical limits of microwave ovens.

6.1 Heat Generation Rate Determination

The three solutions to the heat transfer model described in Chapter 4 were used to determine the temperature distribution within the boehmite and polypropylene layers. It was possible to use the lumped capacitance solution because the approximate Biot number, calculated using Equation (4-36), was found to be approximately 2×10^{-6} . The approximate Biot number assumed that the boehmite was insulated from the polypropylene with

convection on the exterior surface. The Biot number is extremely small because of the micron thickness. Even for the largest expected value of h_{∞} and the smallest possible k , the Biot number would remain insignificantly small. Parameters used in the models are listed in Table 6-1 and Table 6-2: material properties in Table 6-1 and model dimensions and interface conditions in Table 6-2. The heat generation rate \dot{q}_2''' used to compare the model solutions was determined from the finite difference solution. At \dot{q}_2''' equal to 5.5×10^{13} W/m³, 75% of the polypropylene layer was below 150° C when the polypropylene/boehmite interface reached 250° C, according to the finite difference solution. Temperature distributions within the polypropylene and boehmite were also determined at this \dot{q}_2''' for the time the interface reached 250° C (which was different for each model). Two analytical solutions were developed (Figure 6-1 and Figure 6-2), the first using a finite contact conductance of 5000 W/m²·K (Model A) and the other (Model B) using infinite contact conductance (perfect conduction between the two layers). In addition, a finite difference solution (Model C) of the temperature distribution (Figure 6-3) and a lumped capacitance solution (Model D) which calculated the bulk temperature of the boehmite (Figure 6-4) was found. The times for the boehmite at the polypropylene/boehmite interface to reach 250° C and the percentage of the polypropylene under 150° C at that time can be found in Table 6-3 for the four models.

The times required for the boehmite at the interface to reach 250° C are between 10 and 17 μs for all models. Model A and Model D were particularly close. This indicates that with contact resistance (finite contact conductance) between the boehmite and polypropylene the lumped capacitance model is quite accurate, as expected. With significant contact resistance, the boehmite can theoretically be heated without heating the polypropylene (see Model A in Figure 6-1).

The infinite contact conductance (no contact resistance) solutions, Models B and C, allow direct comparison of an approximate cylindrical solution and an approximate cartesian solution. The cartesian solution, (Model B) predicted that a temperature of 229° C would be reached by the boehmite at the interface in 14.6 μs , while the cylindrical solution (Model C) predicted the same temperature would be reached in 13.1 μs . Thus, the cartesian solution lagged the cylindrical solution.

Finally, Models A and B represent upper and lower bounds for the temperature distribution using the approximate analytical solution. In reality the contact conductance lies somewhere between those values but its magnitude is uncertain. No contact conductances for an interface between materials of this type were found in the literature.

6.2 Heat Generation Rate Feasibility

Using \dot{q}_2''' equal to $5.5 \times 10^{13} \text{ W/m}^3$ and Equation (2.8) for microwave power per unit volume

$$\dot{q}_2''' = 8.8 \times 10^{-12} \omega \epsilon'' E_{\text{rms}}^2 \text{ in W/m}^3 \quad (6-1)$$

the E_{rms} required to produce the necessary heat generation rate can be estimated. With $\epsilon'' = 1$ at a frequency of 2.45 GHz, the electric field strength (rms) would need to be 51 MV/m. Since

$$E_{\text{rms}} = \frac{E}{\sqrt{2}} \quad (6-2)$$

the required peak electric field strength E would then be on the order of 71 MV/m. However, the breakdown electric field of air at ambient temperature and pressure at a frequency of 2.45 GHz is 3 MV/m. The breakdown electric field strength is sufficient to break down a gas to its constituents and produce a conducting medium, resulting in discharge. Therefore, since the required electric field is higher than the breakdown field strength, it is impossible to achieve the required field strength.

7. Conclusions and Recommendations

7.1 Conclusions

This research developed a methodology for conducting a feasibility study on the selective microwave heating of a two-layer system and applied it to a candidate system. The study consisted of dielectric property determination, heat transfer modeling, and experimental verification of results. The candidate system involved microwave sol-gel processing of a boehmite coating on a temperature-sensitive polypropylene substrate for a proprietary application.

7.1.1 Development of a Methodology for a Microwave Heating Feasibility Study

The significance of this work lies beyond the microwave heating feasibility study of the boehmite/polypropylene system. The method developed for evaluating the microwave heating feasibility is of more general interest. The method is summarized here. Dielectric property determination is accomplished either through literature review or through experimental methods such as the cavity perturbation technique, which are performed at the expected processing frequency. Microwave heating system requirements are determined through use of the dielectric properties and an order of

magnitude estimate for the heat generation to determine the required field strength. The heat generation is estimated by using appropriate heat transfer models. Experimental verification of the microwave heating feasibility is performed in a microwave applicator.

The following conclusions have been made regarding the developed methodology:

- 1) A successful methodology for performing a microwave heating feasibility study was developed which included dielectric and thermophysical property estimation for all of the materials, determination of the microwave heating system requirements through utilization of heat transfer models of the microwave heating, and experimental microwave heating verification. When applied to a specific problem, the method was able to provide insight into the microwave heating of the two material system. Improvement in the method would be most enhanced by continued improvements in the heat transfer modeling.
- 2) An analytical solution for the transient temperature distribution within a two-material slab, developed using the composite Green's function approach, has been developed and verified. Mathematica®

was used to solve the system of equations. The solution allows for time and spatially dependent heat generation within each material, spatially dependent initial temperature distributions, and contact resistance between the two materials. The solution assumes constant thermophysical and dielectric material properties, assumptions which were acceptable for this feasibility study.

- 3) The heat transfer models developed could be applied to any two material combination and could be expanded to allow more layers (materials) if desired. The methods are general enough that further modifications could be made such as changing of boundary conditions, addition of more layers, or even extending the problem to three-dimensional problems. The only limitation to the application of the method to more complex problems is the ability of Mathematica® (or another similar application for doing mathematics on a computer) to solve the resulting set of equations on the available computer system.

7.1.2 Microwave Heating Feasibility Study for the Boehmite/ Polypropylene System

The following conclusions have been made regarding the feasibility of processing a boehmite coating on a polypropylene substrate:

- 1) Dielectric property measurements of the boehmite using the cavity perturbation technique at 9.4 GHz and experimental heating in a multimode oven indicate that the boehmite can be heated using microwave energy.

- 2) Heat transfer modeling indicated that volumetric heating of a 1 μm boehmite coating to 250° C without degrading the 5 μm diameter polypropylene fiber on which it was coated was theoretically, but not practically, possible. Specifically, the calculated electric field strength was beyond the practical limitations of microwave processing systems.

7.2 Recommendations

With regard to the heat transfer modeling, there are two primary recommendations:

- 1) The approximate analytical solution could be improved by modeling a cylindrical geometry. This would more accurately model the two-layer cylindrical fiber than the plane wall approximation. The same mathematical principles apply; however, the equations would differ. While more computational effort would be necessary to obtain the

solution (if it can be found), the solution would then be exact (at least for constant dielectric and thermophysical properties).

- 2) Investigate means of including temperature dependent dielectric and thermophysical properties in the analytical solution. If this cannot be accomplished with analytical techniques, numerical methods could be used.

As for heating of the boehmite coating on the polypropylene nonwoven, microwave processing would only be feasible if the boehmite were made thicker, made more lossy (dielectrically), and better isolated thermally from the substrate. Possible methods for achieving the latter requirement would be to add an intermediate layer of another material, or to treat the polypropylene to reduce the thermal conductance at the interface with the coating.

References

- Altschuler, H., 1963, "Dielectric Measurements," Handbook of Microwave Measurements, 3rd ed., edited by Sucher and Fox, Polytechnic Press, New York, pp. 495-546.
- ASTM 1991, Annual Book of Standards - Electrical Insulation and Electronics, 1986, "D2520-86, Standard Test Method for Complex Permittivity (Dielectric Constant) of Solid Electrical Insulating Materials at Microwave Frequencies and Temperatures to 1650° C," Vol. 10.02., pp. 214-220.
- Brandrup, J., and Immergut, E.H., 1989, Polymer Handbook, 3rd ed., Wiley, New York.
- Brinker, C.J., and Scherer, G.W., 1990, Sol-gel Science: the Physics and Chemistry of Sol-gel Processing, Academic Press, Boston.
- Bulavin, P.E., and Kashcheev, V.M., 1965, "Solution of the Non-Homogeneous Heat Conduction Equation for Multilayered Bodies," International Chemical Engineering, Vol. 5, No. 1, pp. 112-115.
- Carslaw, H.S. and Jaeger, J.C., 1959, Conduction of Heat in Solids, Clarendon Press, London.
- Chaki, T.K., and Khastgir, D.K., 1990, "Effect of Frequency and Temperature on Dielectric Properties of Polypropylene at X-Band Microwave Region," Journal of Elastomers and Plastics, Vol. 22, January 1990, pp. 58-71.
- Electric Power Research Institute (ERPI), 1987, "Dielectric Heating: RF and Microwave Heating," TechCommentary, Vol. 4, No. 1, pp. 1-4.
- Everhart, Dennis, 1994, Kimberly-Clark, Discussions, April 1994.
- Incropera, F.P, and Dewitt, D.P., 1990, Fundamentals of Heat and Mass Transfer, 3rd. ed., Wiley, New York.
- Jackson, M.L., 1993, "Modeling the Microwave Frequency Permittivity of Thermoplastic Composite Materials," M.S. thesis, Virginia Polytechnic Institute and State University, Blacksburg, VA.

- Lockwood, J.D., and Mulholland, G.P., 1973, "Diffusion through Laminated Composite Cylinders Subjected to a Circumferentially Varying External Heat Flux," Journal of Heat Transfer, Vol. 95c, No. 4, pp. 487-491.
- Ludman, John, 1994, "Evaluation and Design of Polymer Systems for Enhanced Microwave Heating," M.S. thesis, Virginia Polytechnic Institute and State University, Blacksburg, VA.
- Metaxas, A.C., and Meredith, R.J., 1983, Industrial Microwave Heating, Peter Peregrinus, London.
- Mikhailov, M.D., and Özisik, M. N., 1984, Unified Analysis and Solutions of Heat and Mass Diffusion, Wiley, New York.
- Mikhailov, M.D., Özisik, M. N., and Vulchanov, N.L., 1983, "Diffusion in Composite Layers with Automatic Solution of the Eigenvalue Problem," International Journal of Heat and Mass Transfer, Vol. 26, No. 8, pp. 1131-1141.
- Moore, C. H., 1967, "Heat Transfer Across Surfaces in Contact: Studies in Transients in One-Dimensional Composite Systems," Ph.D. dissertation, Mechanical Engineering Department, Southern Methodist University, Dallas, Texas.
- Morse, P.M., and Feshback, H., 1953, Methods of Theoretical Physics, McGraw-Hill, New York.
- Mulholland, G.P., and Cobble, M.N., 1972, International Journal of Heat and Mass Transfer, Vol. 15, pp. 147-160.
- National Bureau of Standards 1979, NBS Monograph 125, *Thermocouple Reference Tables*, Washington, D.C.
- Özisik, M.N., 1968, Boundary Problems of Heat Conduction, International Textbook, Scranton, PA.
- Özisik, M.N., 1993, Heat Conduction, 2nd, ed., Wiley, New York.
- Portier, J.J., and Arnas, O.A., 1975, "Analytical Study of Unsteady Heat Conduction in Composite Regions," Proceedings: 3rd. International Conference on Structural Mechanics in Reactor Technology, Vol. 5, Part L, Section 1/5, pp. 1-10.

Poulikakos, D., 1994, Conduction Heat Transfer, Prentice Hall, Englewood Cliffs, New Jersey.

Pozar, D., 1990, Microwave Engineering, Addison-Wesley, New York.

Stern, C.H., 1994, "Microwave Processing of Nonwovens: An Introduction," International Nonwovens Journal, Vol. 6, No. 3, pp. 43-49.

Von Hippel, A., 1954, Dielectrics and Waves, M.I.T. Press, Cambridge, Massachusetts.

White, J.R., 1970, "Measuring the Strength of the Microwave Field in a Cavity," Journal of Microwave Power, Vol. 5, No. 2, pp. 145-147.

Table 3-1 WR-90 Resonant Cavity Components

Component	Resonant Frequency = 9.4 GHz
Straight Section	Custom (Oak Ridge National Laboratory)
Coax to Waveguide Transition	Maury Microwave Model X209D2
Iris	0.267" Dia. 0.0056" Thick
Shorting Plate	Custom 1/4" Thick Polished Aluminum

Table 3-2 Dielectric Properties of Selected Materials at Microwave Frequencies (Stern 1994)

Dielectric Properties of Selected Materials at Microwave Frequencies
(Relative to the permittivity of free space, $\epsilon_0 = 8.8 \times 10^{-12} \text{ F/m}$)

Material	Frequency MHz	Temp. °C	Diel. Const. ϵ'	Loss Factor ϵ''
Water ⁷ —Distilled	3000	25	76.7	12.0
—+0.5 molal NaCl	3000	95	52	2.4
—Ice (pure)	3000	25	67	41.9
Glass —Pyrex ⁷	3000	-12	3.2	0.003
—Fused quartz ⁷	3000	25	4.82	0.026
Teflon (PTFE) ⁷	3000	25	3.78	0.0002
Acetate ⁷	3000	22	2.1	0.0003
Acrylic: thermoplastic, cast ¹⁴	3000	25	3.2	0.09
Nylon 66 ⁷	3000	20	2.6	0.0013
Polyester:	3000	25	3.03	0.039
Resin, Mylar ⁶	1000	20	2.2	0.0088
Polyethylene terephthalate (PET) film ¹⁵	1000	23	2.8	0.0084
Polyethylene ⁷	3000	24	2.25	0.0007
Polypropylene ¹⁵	1000	-	2.4	0.003
Wool Fiber: 7% Moisture content (dry) ⁶	3000	-	3.9	0.29

Table 5-1: Dimensional Values for Test Cases

Material Properties (Boehmite)

$$\alpha = 8.21 \times 10^{-7} \text{ m}^2/\text{s}$$

$$k = 2.1 \text{ W}/(\text{m K})$$

Convection Heat Transfer Coefficient

$$h_c = 50 \text{ W}/(\text{m}^2 \text{ K})$$

89

Length

$$L = 0.05 \text{ m}$$

$$R = 2 L$$

Number of Terms in Composite Green's Function

$$n = 5$$

Table 6-1: Material Properties for the Heat Transfer Models

	Boehmite (Dried Sol-Gel)	Polypropylene (Bulk)
Density ρ (Dry) (kg/m ³)	3010	900
Thermal Conductivity k (W/m·K)	2.1	0.117
Specific Heat c_p (J/kg·K)	850	1926
Source	Approximate, Kimberly-Clark	<u>Polymer Handbook</u>

Table 6-2: Model Geometry and Interface Conditions Comparison

	Approximate Analytical Solution (Contact Resistance) Model A	Approximate Analytical Solution Model B	Finite Difference Solution Model C	Lumped Capacitance Solution Model D
Coordinate System	Cartesian (Figure 4-3)	Cartesian (Figure 4-3)	Cylindrical (Figure 4-4)	N/A (Figure 4-4)
h ($W/m^2 \cdot K$)	0	0	0	5
h_c ($W/m^2 \cdot K$)	5000	∞	N/A	N/A
t_{Boehmite} (μm)	$L_2 - L_1$	$L_2 - L_1$	$R_2 - R_1$	1.00
L_1 (μm)	1.25	1.25	N/A	N/A
L_2 (μm)	2.25	2.25	N/A	N/A
R_1 (μm) ($=2 L_1$)	N/A	N/A	2.50	N/A
R_2 (μm) ($=L_1+L_2$)	N/A	N/A	3.50	N/A
Number of terms, n	5	5	N/A	N/A
Number of Nodes (n , n)	N/A	N/A	121, 81	N/A
Weight Factor, λ	N/A	N/A	0.5	N/A
ΔT (ns)	N/A	N/A	10	N/A

	Model Solution	Time (μ s) Until Boehmite at Interface Reaches 250° C	% of Polypropylene Under 150° C
A	Analytical, $h_c = 5000 \text{ W/m}^2 \cdot \text{K}$	10.6	100
B	Analytical, $h_c = \infty$	16.2	45
C	Finite Difference	14.6	75
D	Lumped Capacitance	10.5	N/A

Table 6-3: Comparison of Model Solutions Using $\dot{q}_2''' = 5.5 \times 10^{13} \text{ W/m}^3$

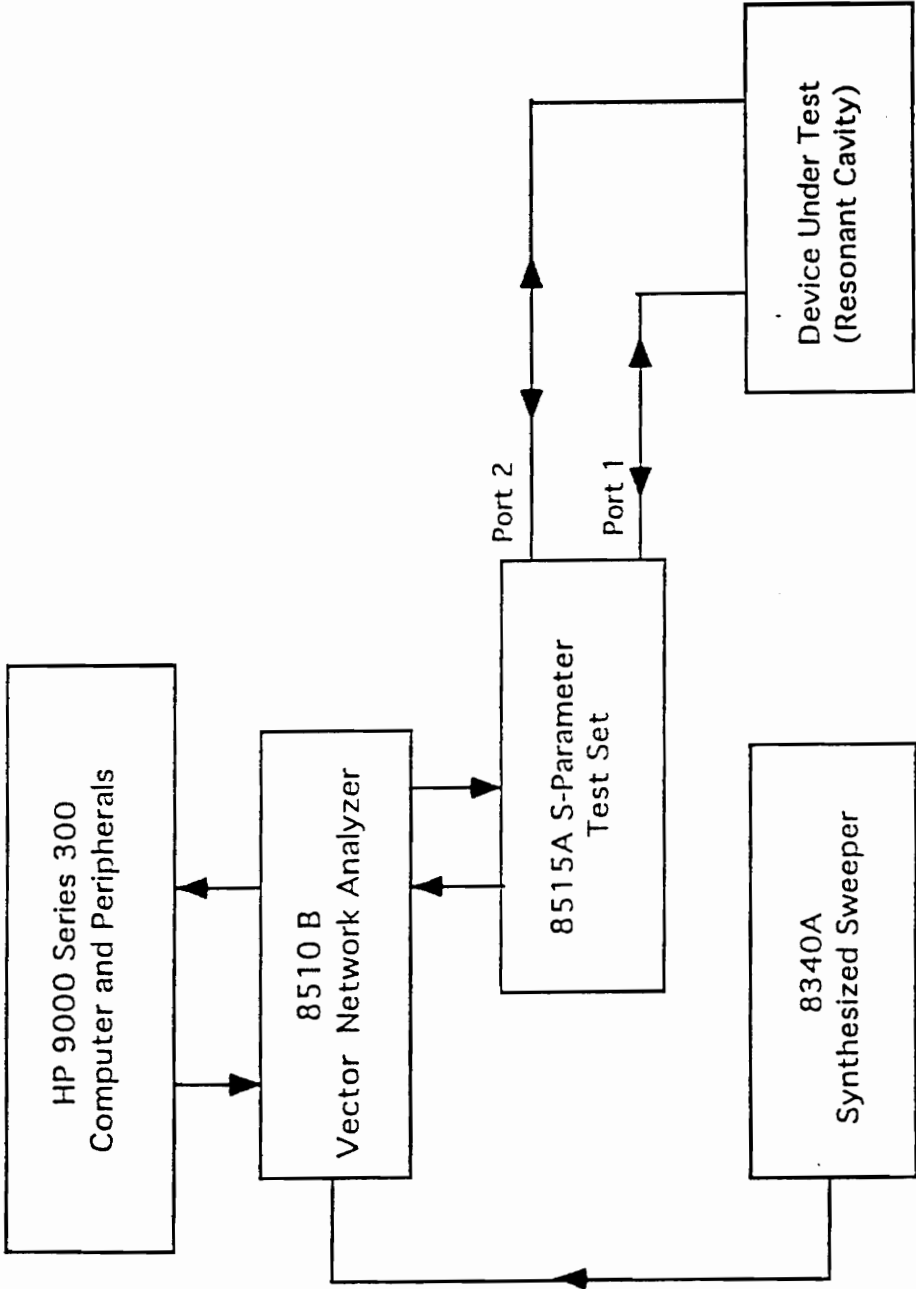


Figure 3-1 Schematic of the Hewlett-Packard 8510B Network Analyzer System (Jackson 1993)

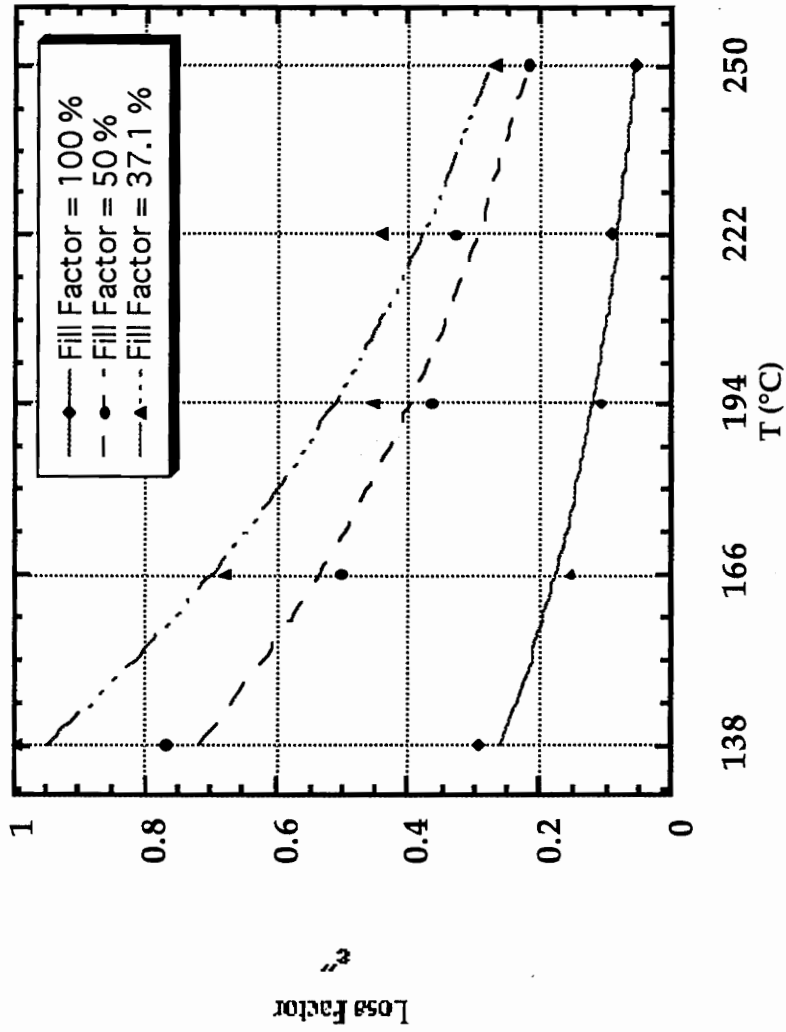


Figure 3-2 Loss Factor (ϵ'') at 9.4 GHz of Boehmite Dried for One Hour in Oven at Temperature T . (ϵ'' measurements made at room temperature)

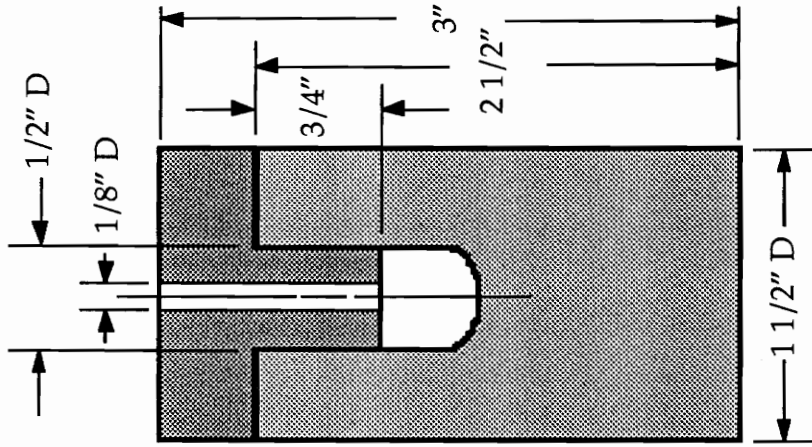


Figure 3-3 Low-Loss, Teflon, Cylindrical Sample Holder

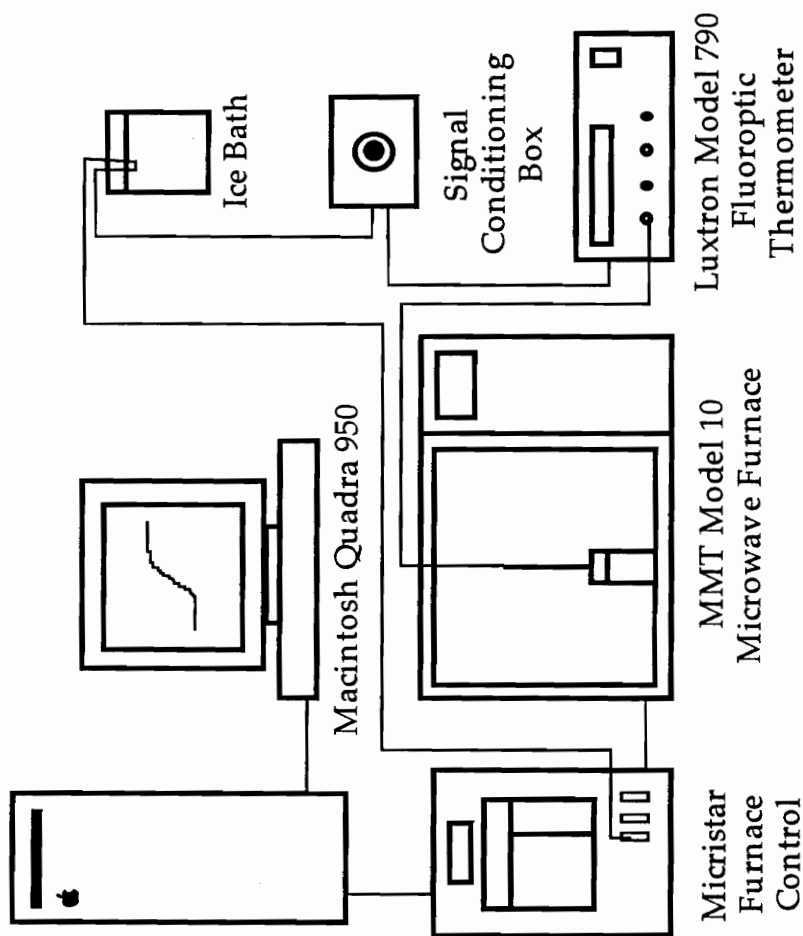


Figure 3-4 Schematic of the Multimode Oven System

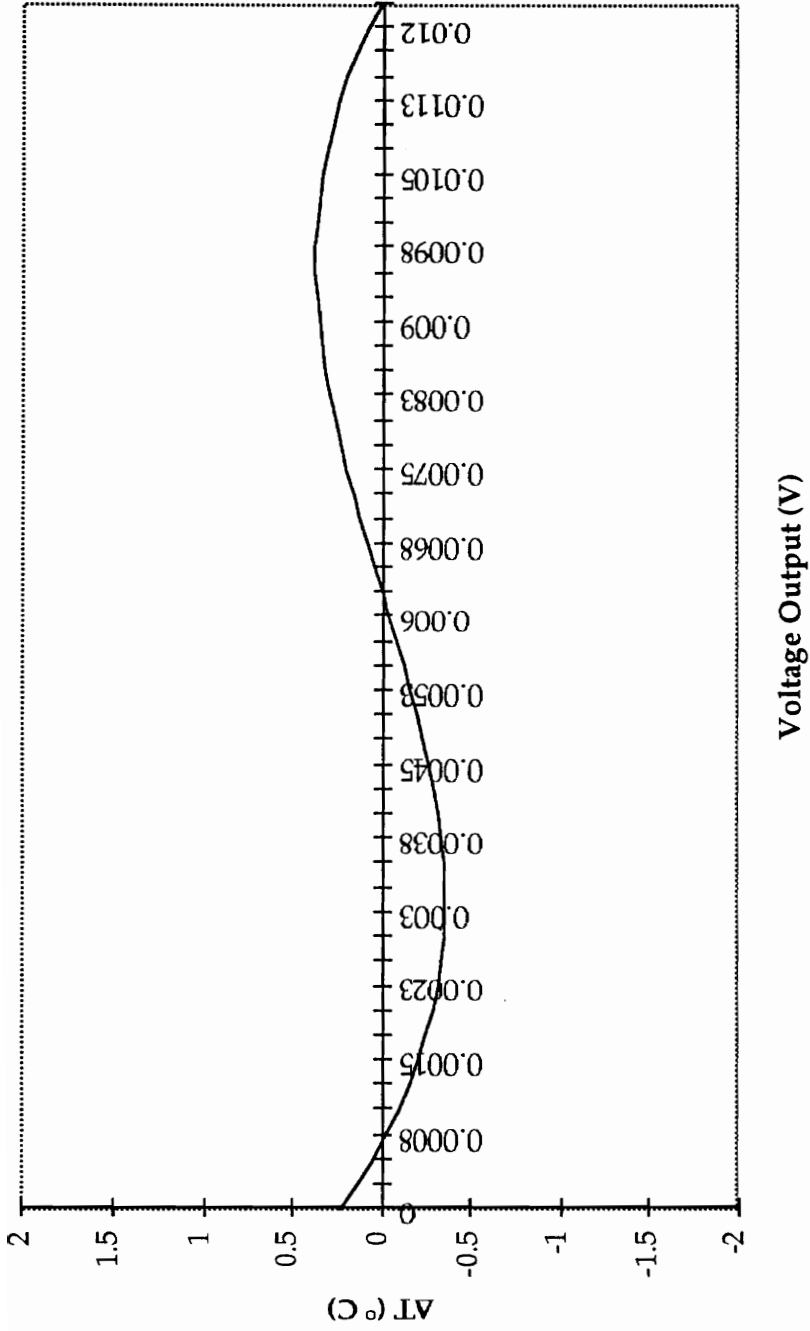


Figure 3-5 Deviation ΔT of Type K Thermocouple Temperature from being a Linear Function of Voltage Output Between 0 and 300° C (0 mV to 12.25 mV)

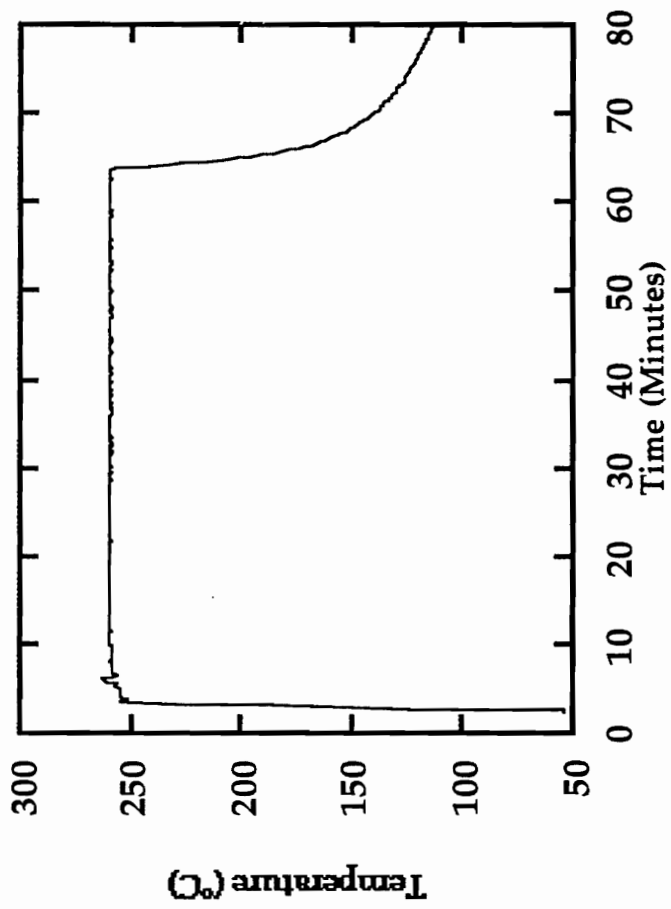


Figure 3-6 Microwave Heating of Boehmite Sol-Gel. One hour at 260° C

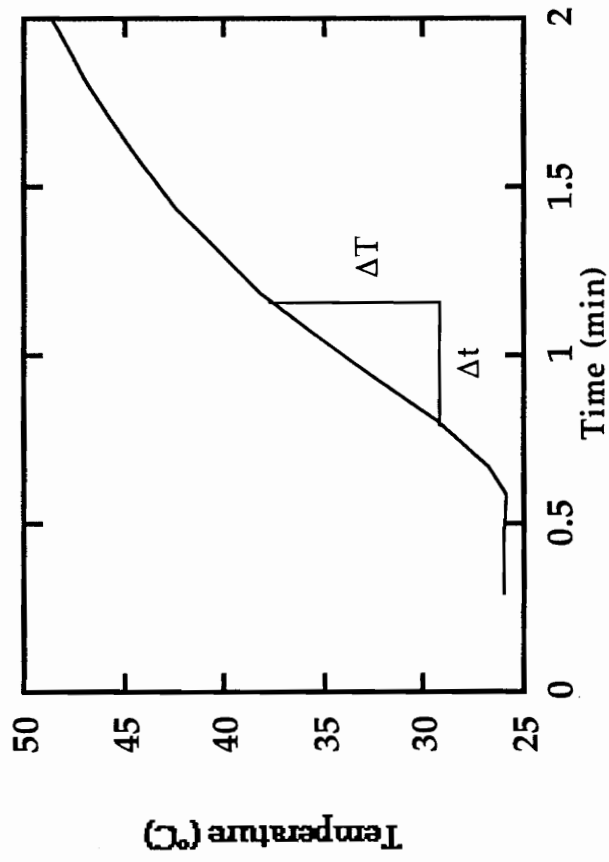


Figure 3-7 E_{rms} Determination Data. Microwave Heating of Crushed Pyrex Glass at 60 % Power

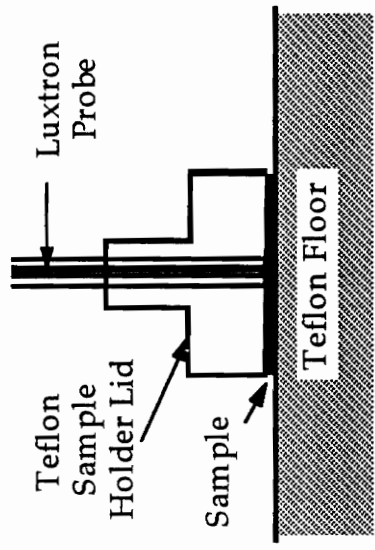


Figure 3-8 Configuration for the Microwave Heating of a Boehmite Coated Nonwoven

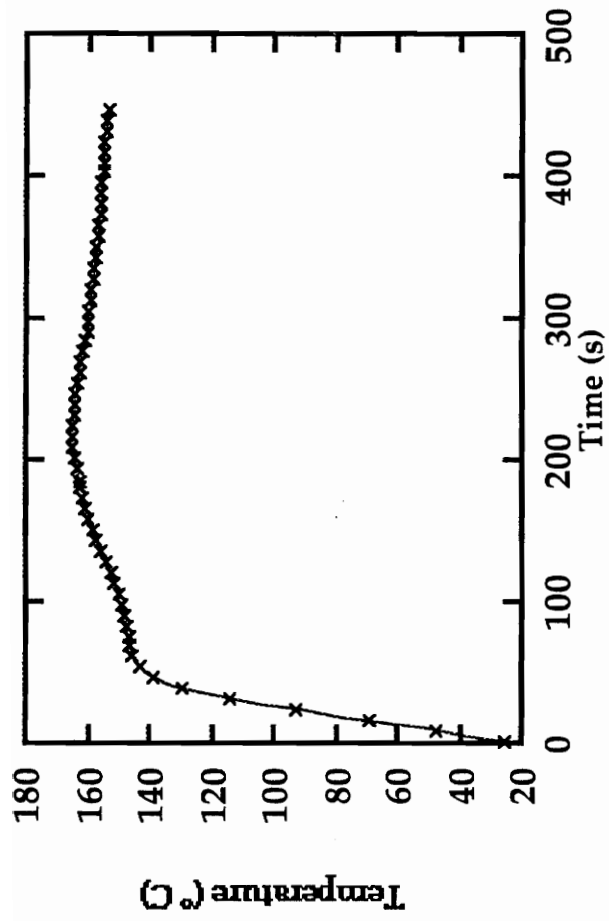


Figure 3-9 Temperature Profile for Microwave Heating of a Boehmite Coated Nonwoven

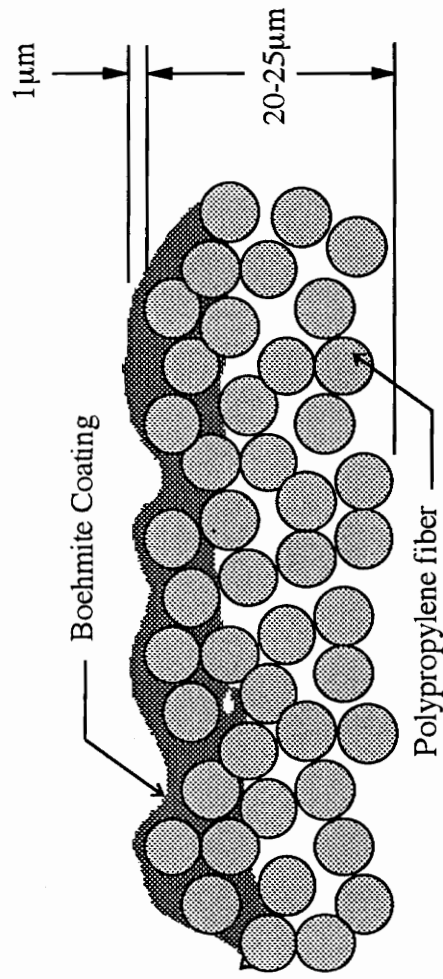


Figure 4-1 Physical Model of Polypropylene Nonwoven with Boehmite Coating

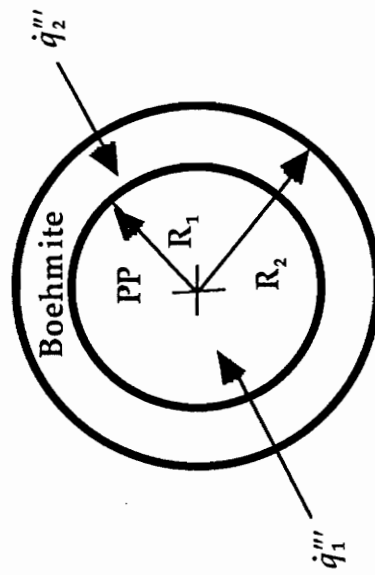
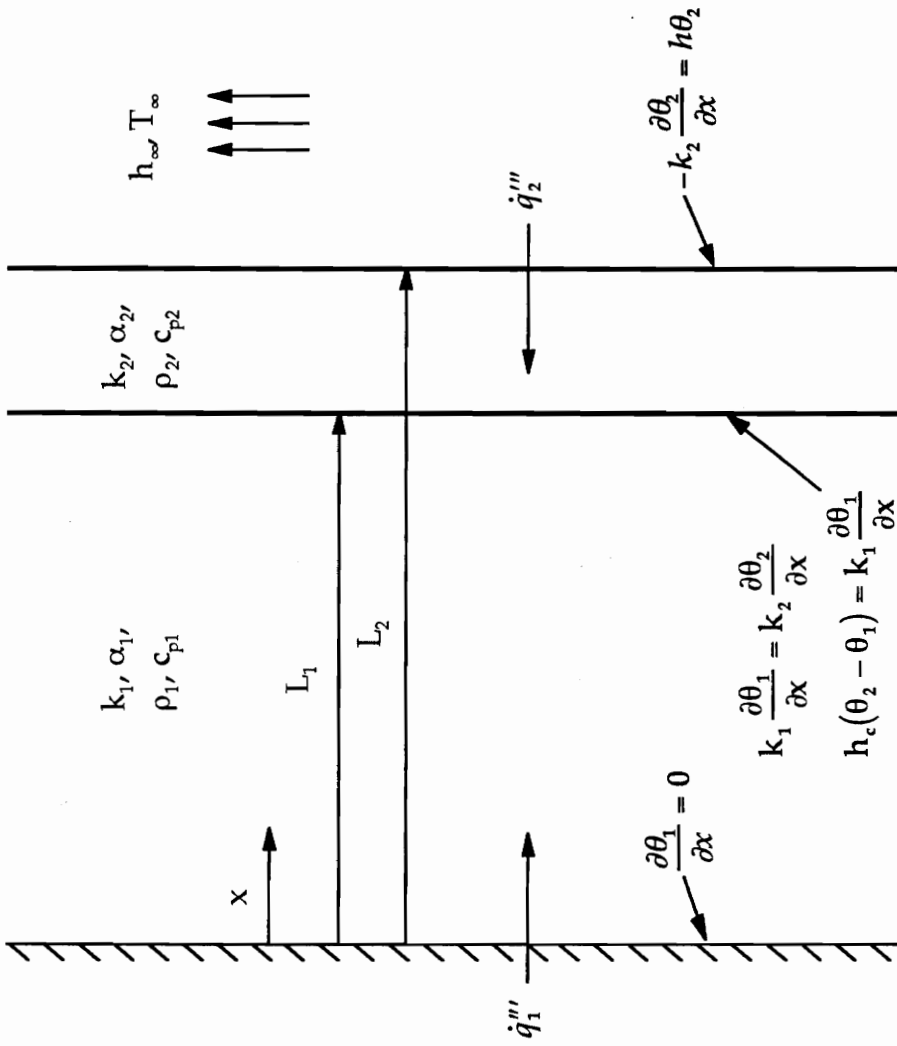
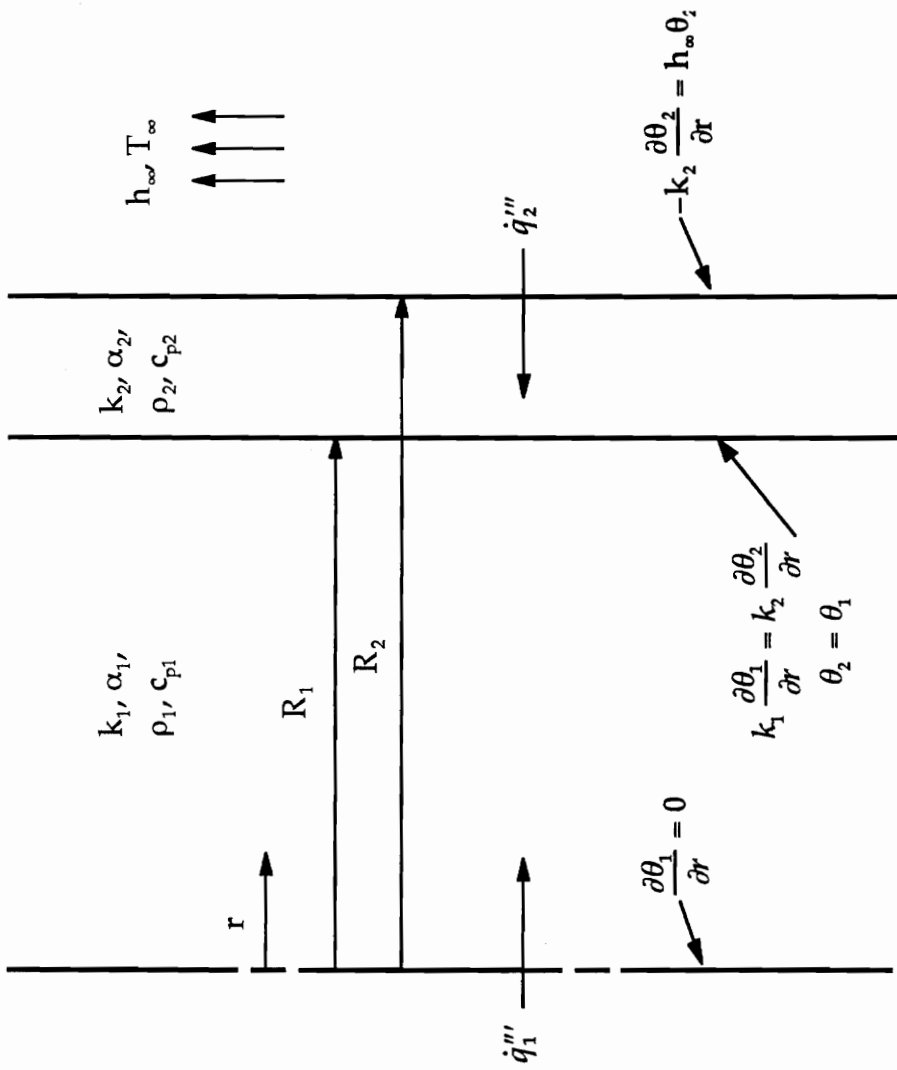


Figure 4-2 Geometry for the Long Polypropylene Fiber Coated with Boehmite



where $\theta_1(x,t) = T_i(x,t) - T_\infty$ and $\theta_2(x,t) = T_o(x,t) - T_\infty$

Figure 4-3 Geometry of the Approximate Analytical Green's Function Solution



where $\theta_1(r,t) = T_1(r,t) - T_\infty$ and $\theta_2(r,t) = T_2(r,t) - T_\infty$

Figure 4-4 Geometry of the Cylindrical Finite Difference Solution

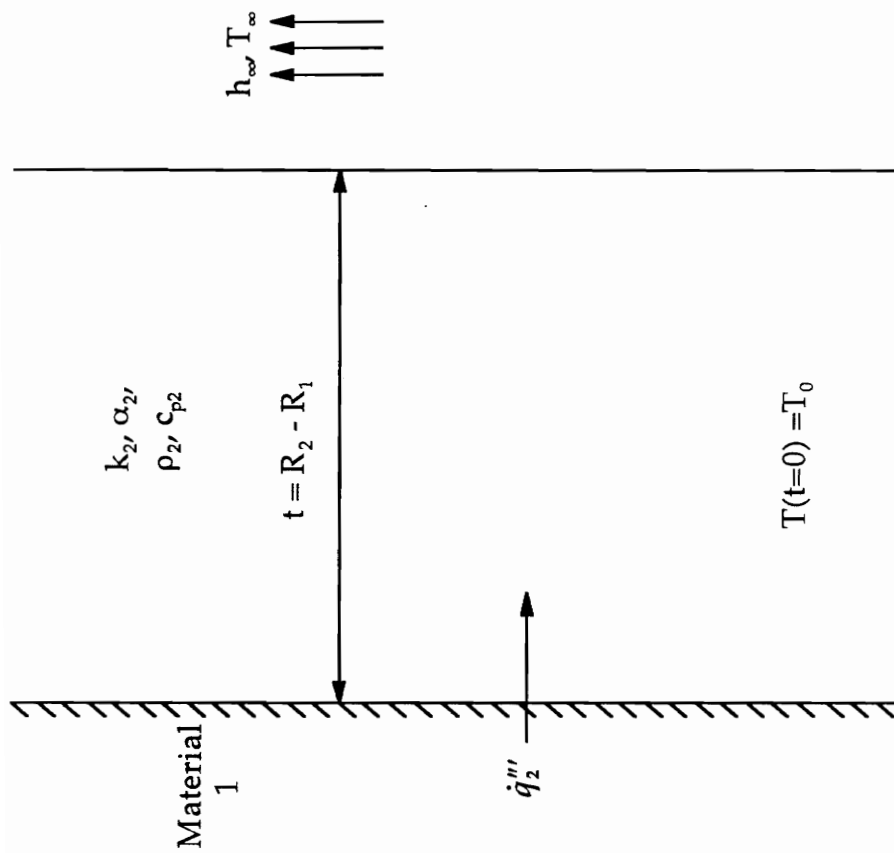


Figure 4-5 Geometry of the Lumped Capacitance Solution

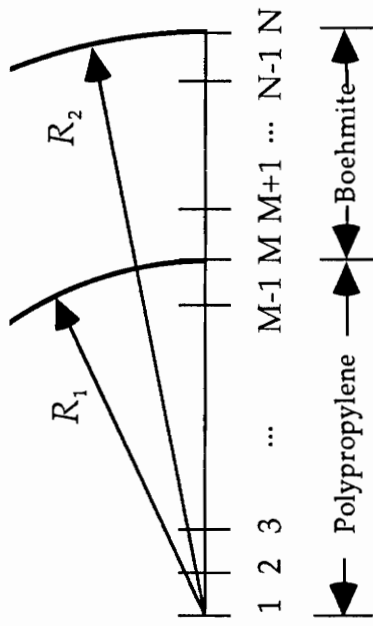


Figure 4-6 Finite Difference Model Nodes

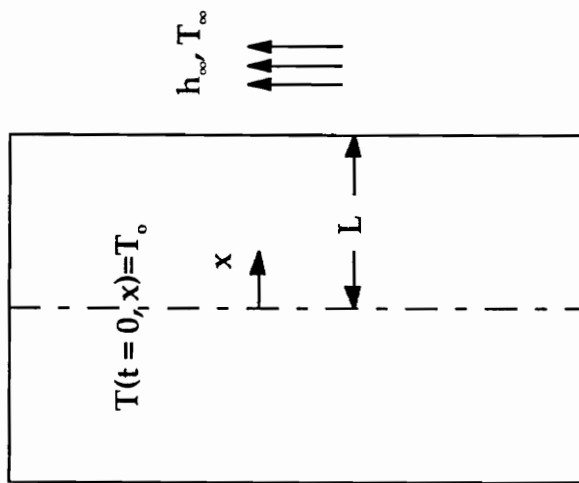


Figure 5-1 Geometry of Test Case 1

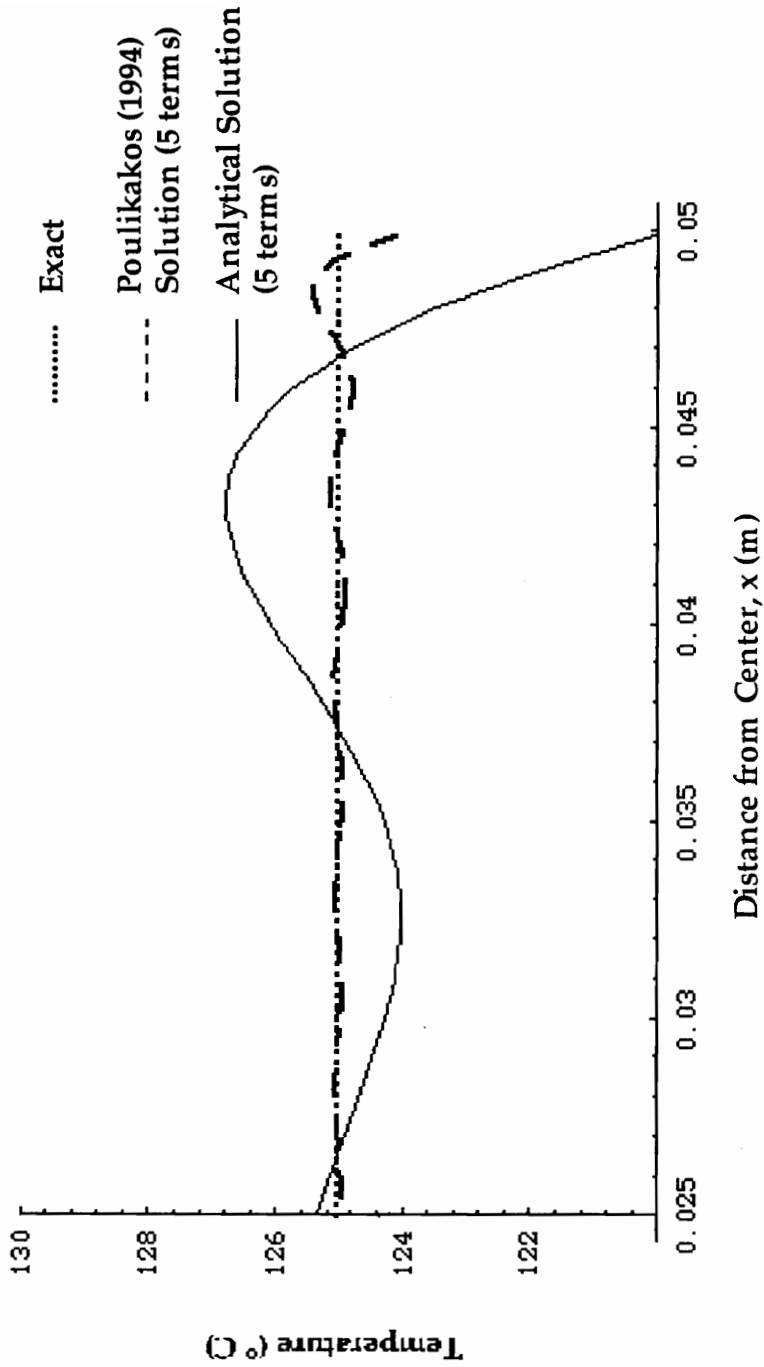


Figure 5-2 Test Case 1: Detail of Solutions at $t = 0$

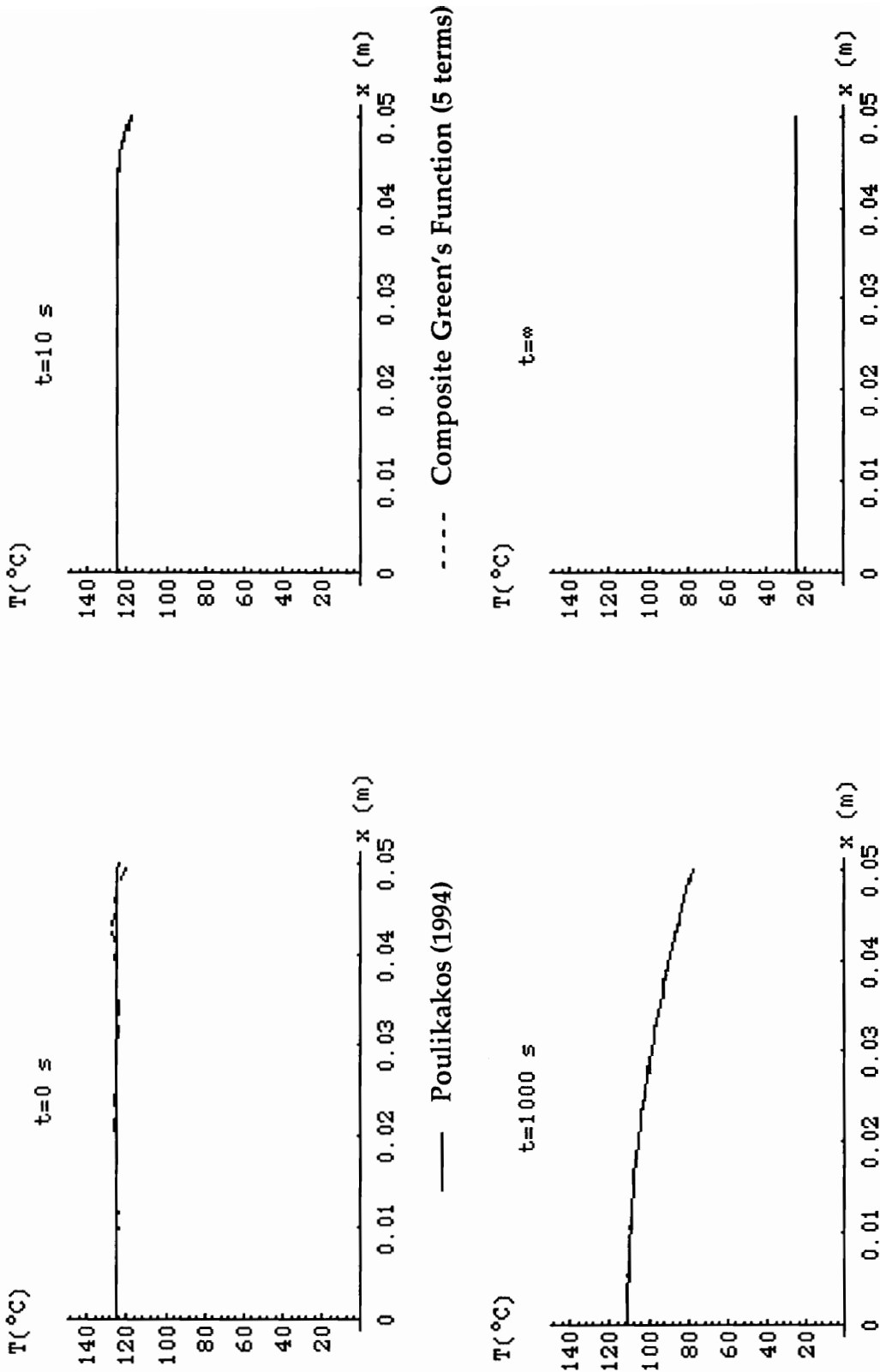


Figure 5-3 Test Case 1: Comparison of Solutions to Initial Condition Problem

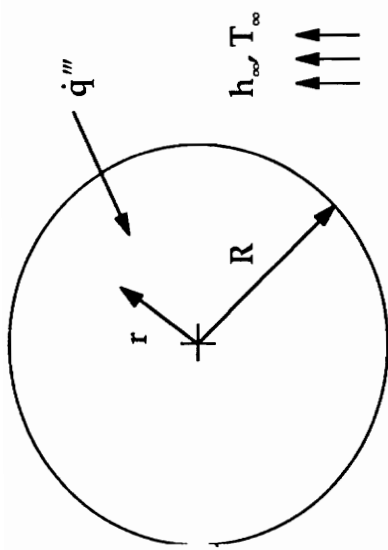


Figure 5-4 Geometry of Test Case 2

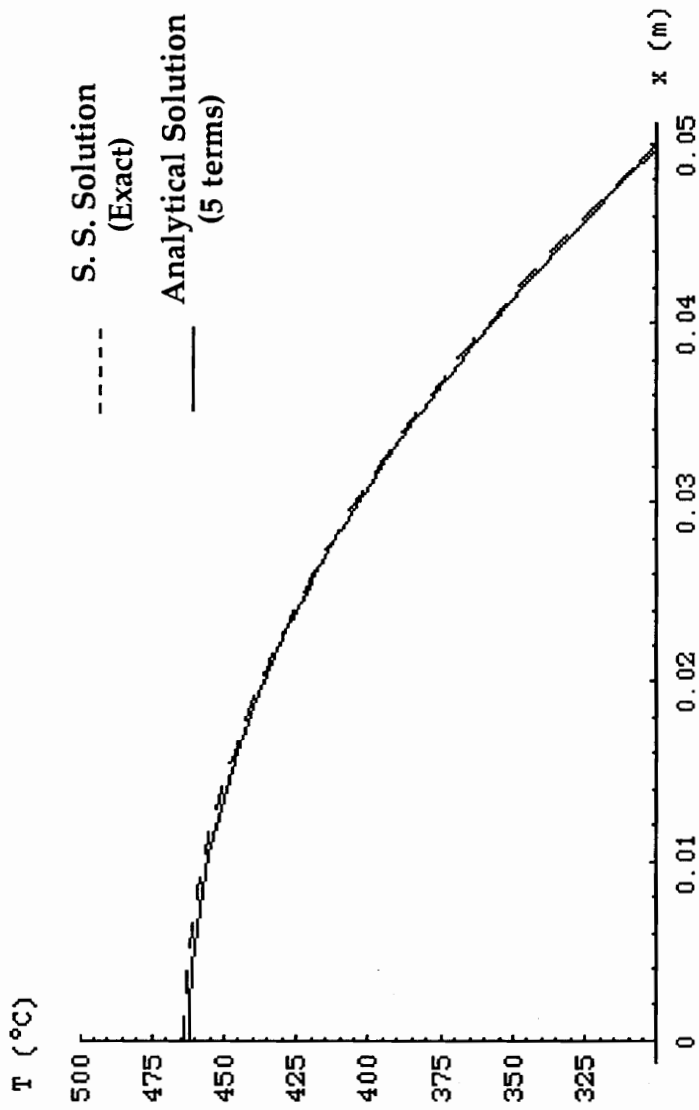


Figure 5-5 Test Case 2: Comparison Between the Temperature Distribution of the Analytical Model at Steady State and Expected Values

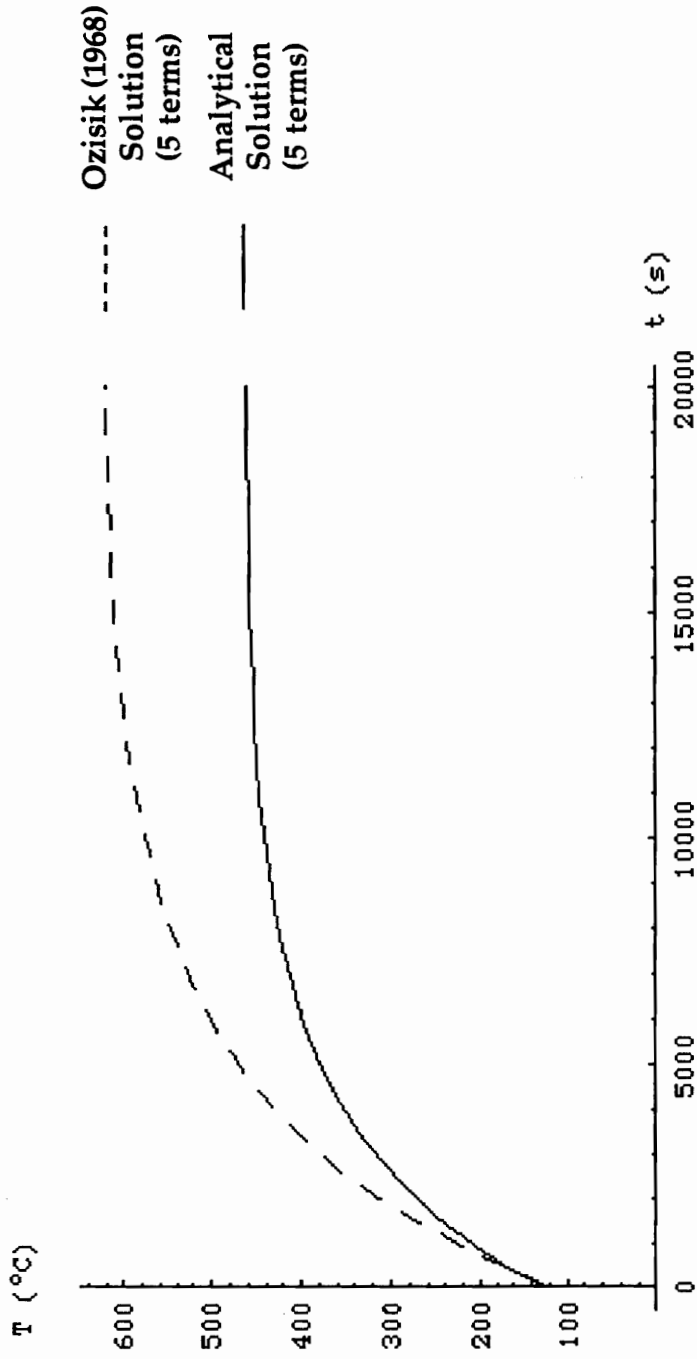


Figure 5-6 Test Case 2: Comparison between Transient Temperature Distributions of the Analytical Model at $x = 0$ and the Ozisik Solution at $r = 0$

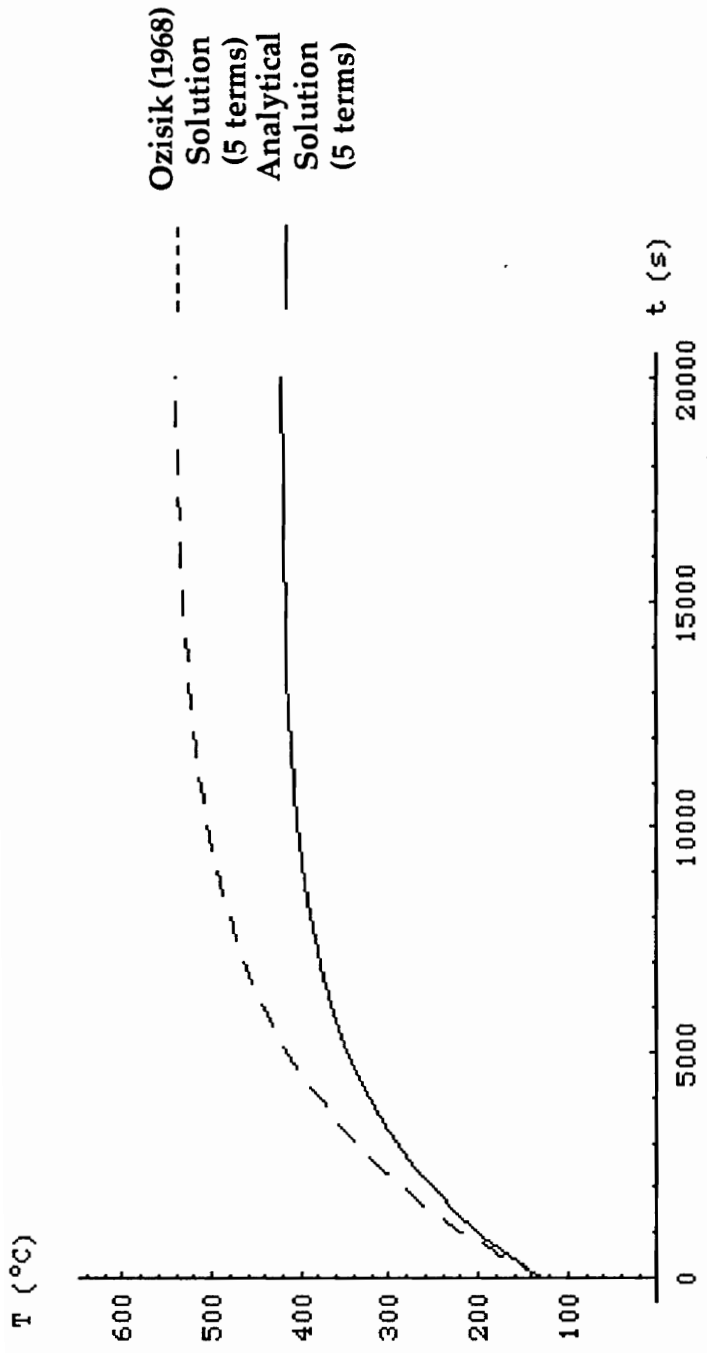


Figure 5-7 Test Case 2: Comparison between Transient Temperature Distributions of the Analytical Model at $x/L = 1/2$ and the Ozisik Solution at $r/R = 1/2$

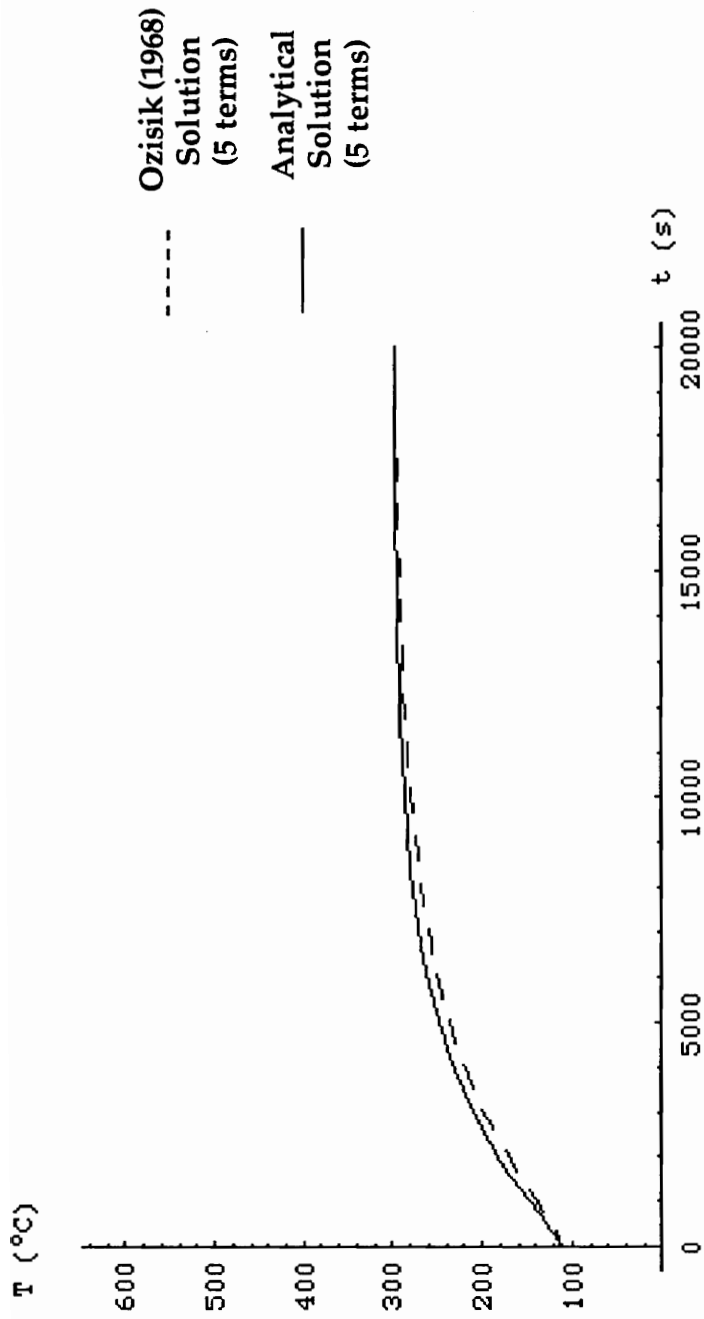


Figure 5-8 Test Case 2: Comparison between Transient Temperature Distributions of the Analytical Model at $x/L = 1$ and the Ozisik Solution at $r/R = 1$

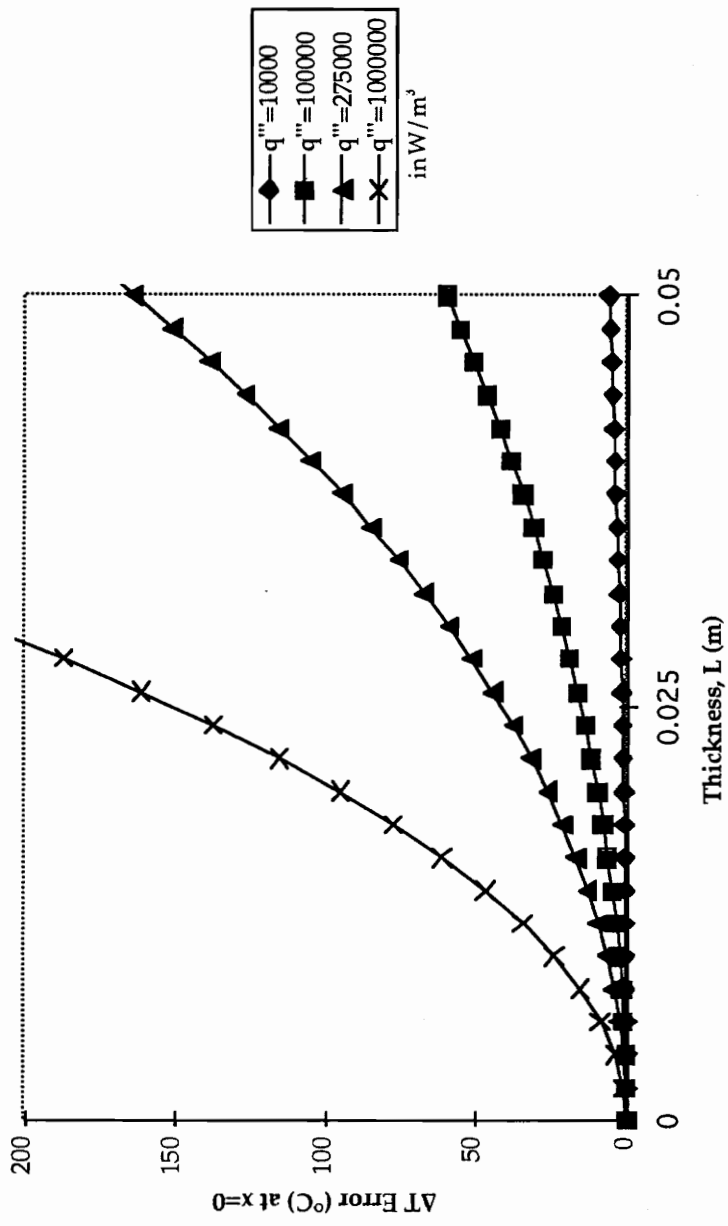


Figure 5-9 Maximum Temperature Error for the Cartesian (Plane Wall) Solution of Test Case 2

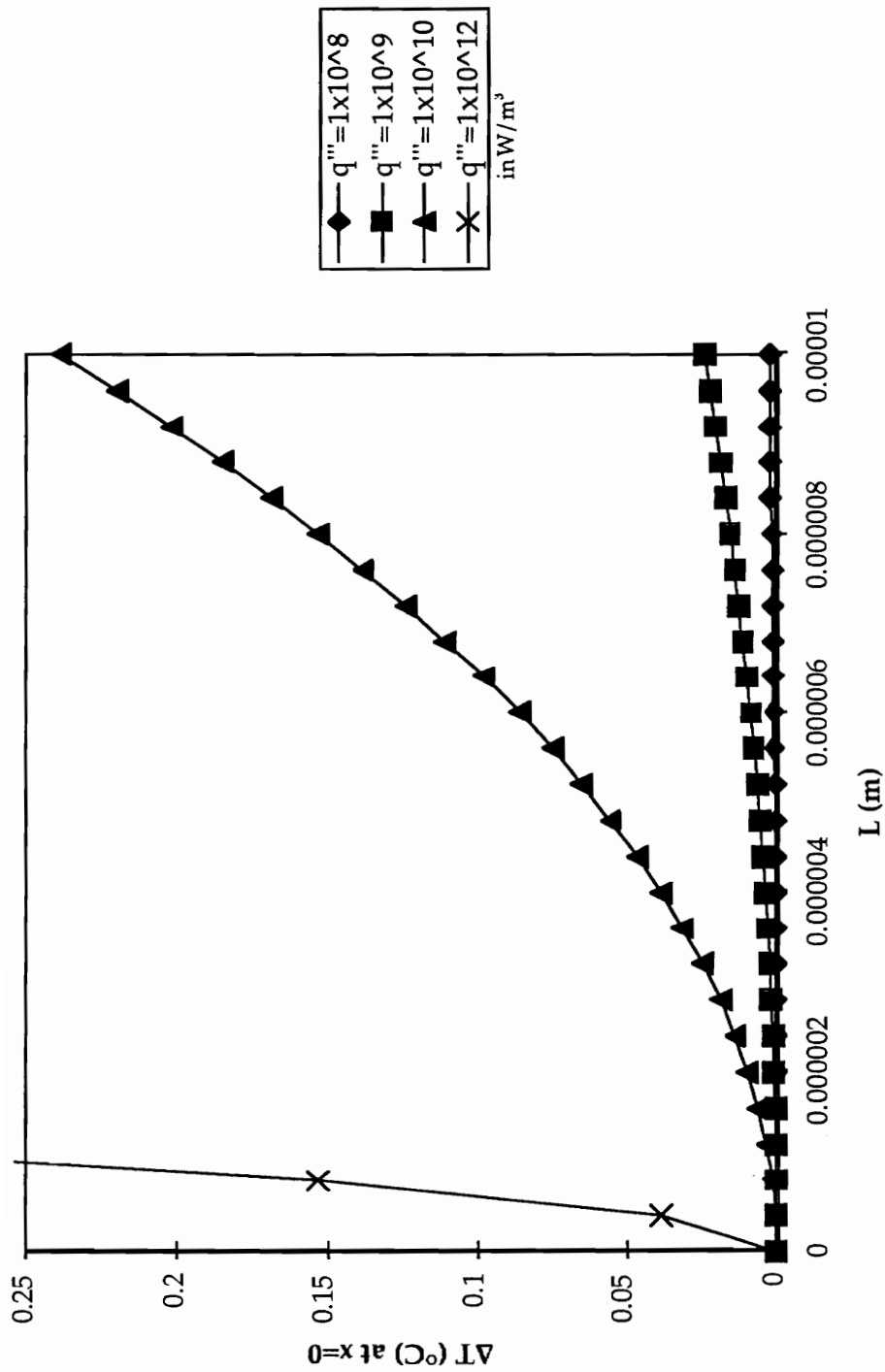


Figure 5-10 Maximum Temperature Error for Cartesian (Plane Wall) Model at Micron Thicknesses

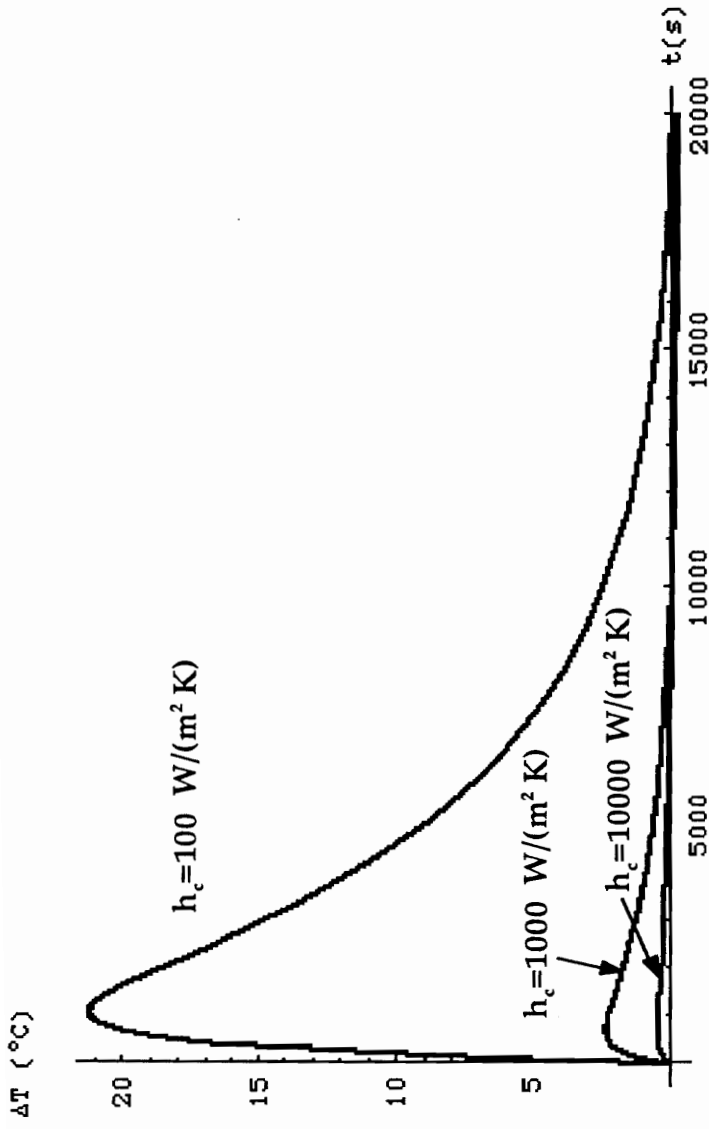


Figure 5-11: Test Case 3: Temperature Difference at the Interface over Time as a Function of the Contact Conductance h_c

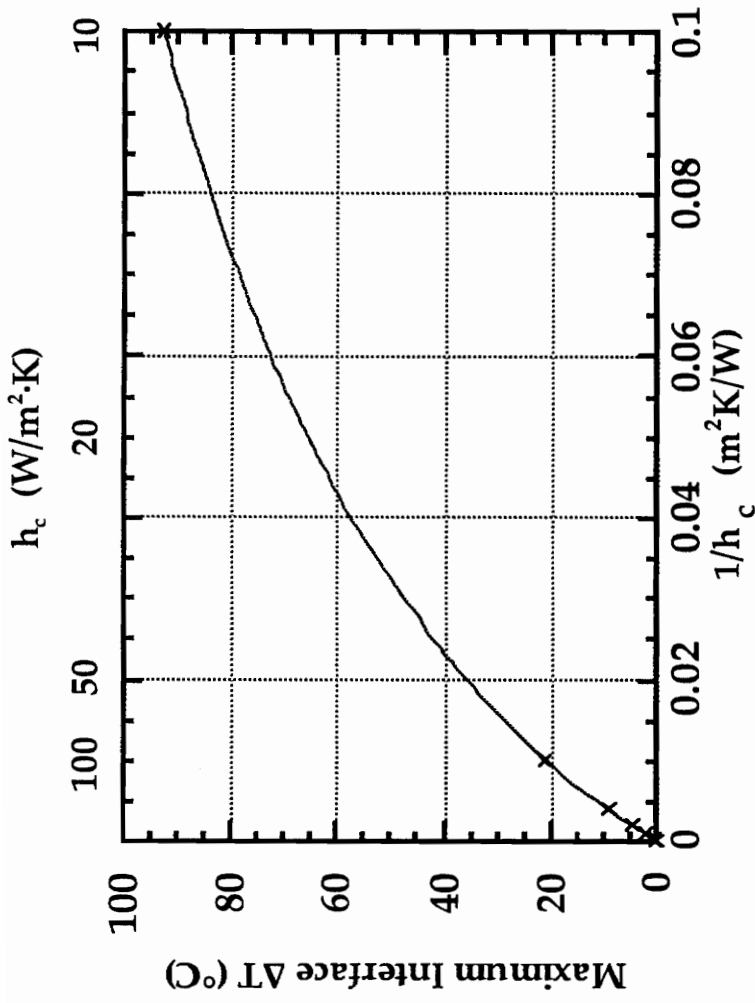


Figure 5-12: Maximum Temperature Difference at the Interface as a Function of the Contact Conductance h_c

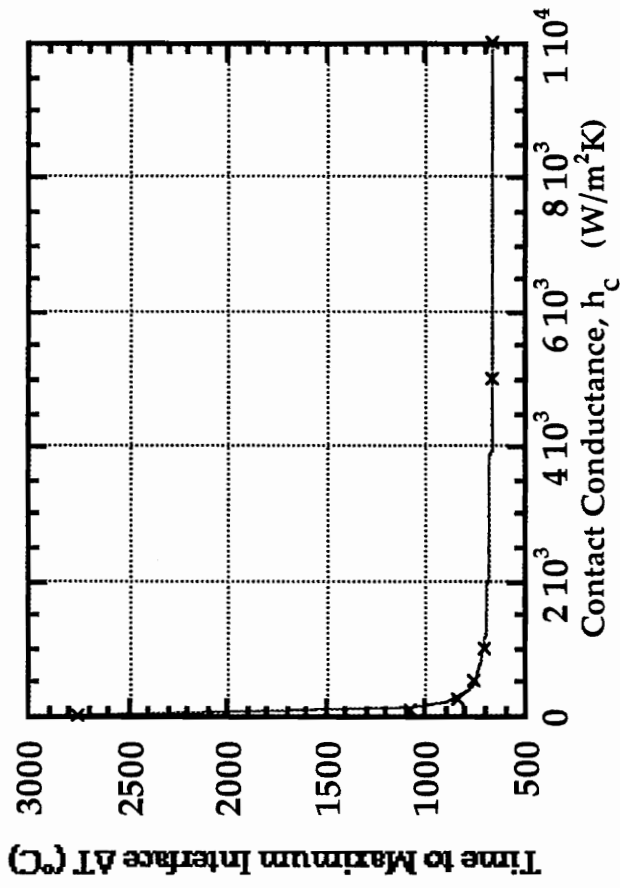
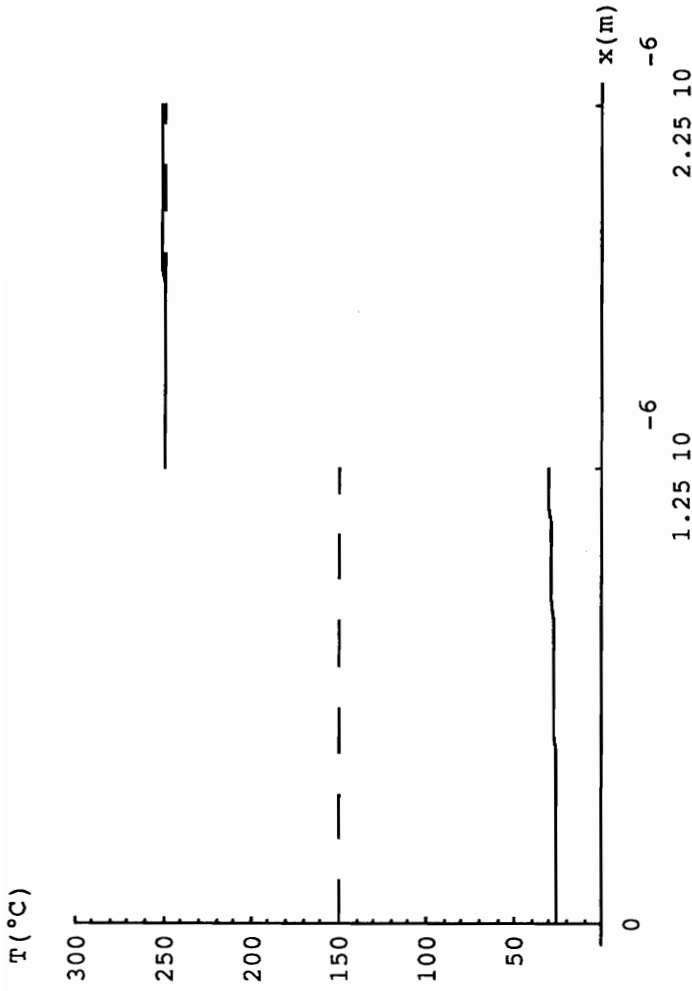
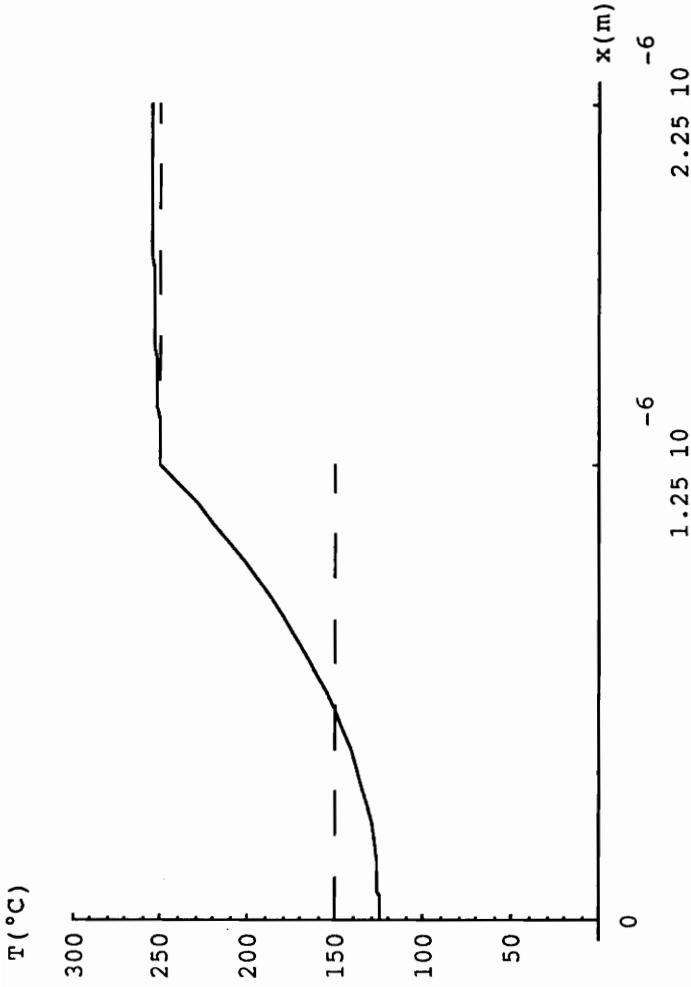


Figure 5-13: Test Case 3: Time to Maximum Interface ΔT as a Function of the Contact Conductance h_c .



Note: Dashed lines indicate desired temperature distribution. Solid lines indicate model results.

Figure 6-1: Temperature Distribution at $t = 10.6 \mu\text{s}$ Using the Approximate Analytical Solution with $h_c = 5000 \text{ W / m}^2 \cdot \text{K}$ (Model A)



Note: Dashed lines indicate desired temperature distribution. Solid lines indicate model results.

Figure 6-2: Temperature Distribution at $16.2 \mu\text{s}$ Using the Approximate Analytical Solution with $h_c = \infty$ (Model B)

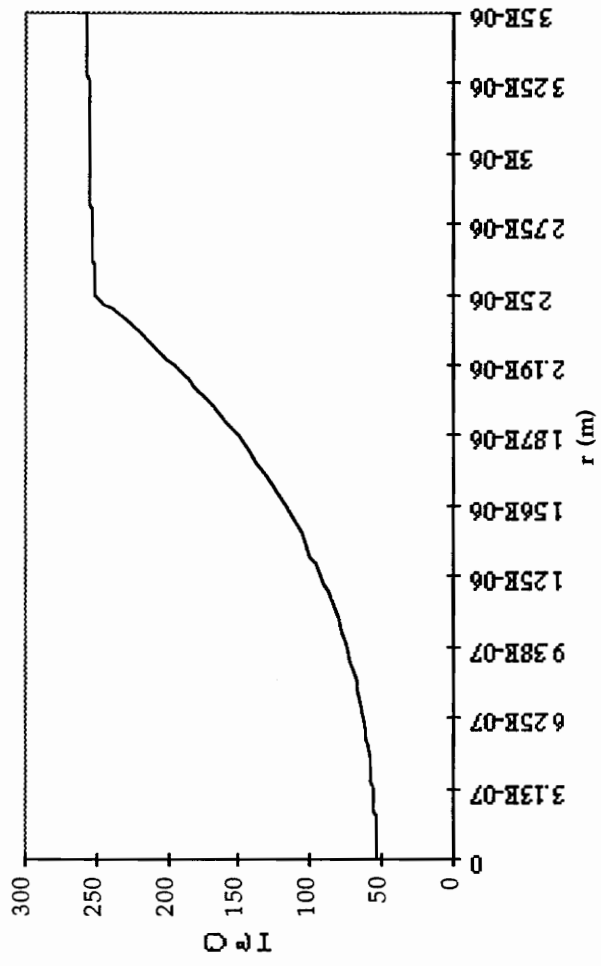


Figure 6-3 Temperature Distribution at 14.6 μ s Using the Finite Difference Solution (Model C)

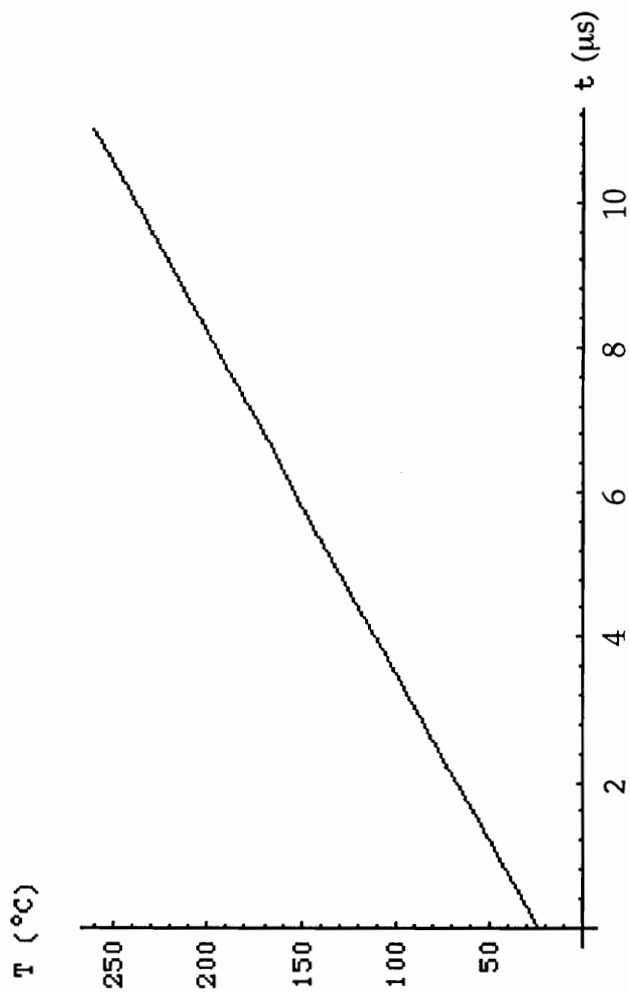


Figure 6-4: Bulk Temperature Over Time Using the Lumped Capacitance Solution (Model D)

A. Approximate Analytical Solution - Mathematica Programs

Following are three files from Mathematica used to develop the approximate analytical solution. In A.1, the eigenvalues β_n are computed. In A.2, the β_n values are used in the computation of the temperature distributions $T_i(x,t)$. In A.3, an output file is presented which takes the temperature distribution output from A.2 to produce the desired numerical and graphical information.

A.1 Eigenvalue Determination Program

```
B[n_] := B[n]
alpha1 = 6.7497 * 10^-8;
alpha2 = 8.2079 * 10^-7;
k1 = 0.117;
k2 = 2.1;
L1 = 1.25 * 10^-6;
L2 = 2.25 * 10^-6;
hinf = 0.0001;
h2c = Infinity;
a1 = B/alpha1^0.5;
a2 = B/alpha2^0.5;
gamma = a1 L1;
eta = a2 L2;
k = k1/k2;
a = (alpha2/alpha1)^0.5;
h1 = k1/h2c;
h2 = k2/hinf;
l = L1/L2;
```

Find $\det[m] = 0$ for $B[n]$ determination - B in following eqns

```
m = {{h1 a1 Sin[gamma] - Cos[gamma], Sin[l eta],
      Cos[l eta]}, {k a Sin[gamma], Cos[l eta], -Sin[l eta]},
      {0, h2 a2 Cos[eta] + Sin[eta], -h2 a2 Sin[eta] +
      Cos[eta]}};
```

```

Det[m];
det=%;
Plot[det, {B, 0, 5000}];
Plot[det, {B, 0.0, 0.0004}];
Plot[det, {B, 0, 100}];
Plot[det, {B, 0, 500}];
Plot[det, {B, 500, 1000}];
Plot[det, {B, 1500, 2000}];
Plot[det, {B, 2000, 2500}];
Plot[det, {B, 2500, 3000}];
Plot[det, {B, 3500, 4000}];
Plot[det, {B, 4000, 4500}];
Plot[det, {B, 4500, 5000}];
Plot[det, {B, 5500, 6000}];
Plot[det, {B, 6500, 7000}];
Plot[det, {B, 7500, 8000}];
Plot[det, {B, 5000, 10000}];
bet = B[i], i= 1, n
bet={FindRoot[det == 0, {B, 0.004}],
FindRoot[det == 0, {B, 400}],
FindRoot[det == 0, {B, 1000}],
FindRoot[det == 0, {B, 1600}],
FindRoot[det == 0, {B, 2200}],
FindRoot[det == 0, {B, 2800}],
FindRoot[det == 0, {B, 3000}],
FindRoot[det == 0, {B, 3600}],
FindRoot[det == 0, {B, 4200}],
FindRoot[det == 0, {B, 4800}],
FindRoot[det == 0, {B, 5400}],
FindRoot[det == 0, {B, 5800}],
FindRoot[det == 0, {B, 6200}],
FindRoot[det == 0, {B, 6900}],
FindRoot[det == 0, {B, 7600}],
FindRoot[det == 0, {B, 8100}],
FindRoot[det == 0, {B, 8600}],
FindRoot[det == 0, {B, 8900}],
FindRoot[det == 0, {B, 9500}],
FindRoot[det == 0, {B, 10100}]}];
B/.%;

```

A.2 Temperature Distribution Determination Program

Transient Temperature Distribution in a 1-D, Two
Material Sytem with Internal
Heat Generation in Material 2

```
Define b[n], Aln[n], Bln[n], A2n[n], B2n[n,case],  
1≤n≤nterm, case: h2c=5000
```

```
B[n_]:=B[n]  
alpha1=6.7497*10^-8;  
alpha2=8.2079*10^-7;  
k1=0.117;  
k2=2.1;  
L1=1.25*10^-6;  
L2=2.25*10^-6;  
hinf=0.0001;  
h2c=Infinity;  
Tinf=25;  
a1=B/alpha1^0.5;  
a2=B/alpha2^0.5;  
gamma=a1 L1;  
eta=a2 L2;  
kk=k1/k2;  
a1=(alpha2/alpha1)^0.5;  
h1=k1/h2c;  
h2=k2/hinf;  
l=L1/L2;  
nterm=5;
```

b = the list output from file "Eigenvalues h2c=..."

```
beta[n_]:=beta[n]  
b={0.00460030383998412585, 406.2485943971533679,  
999.7399653044818972, 1623.316854567456335,  
2235.730231775566107,  
2731.96729664945287, 3073.230364086419891,  
3625.663942712559822,
```

```
4245.267798456649317, 4866.12272327654677,  
5430.02010549245733,
```

```
5780.177932535048563, 6257.826743296587393,  
6867.34420369958012,
```

```
7491.228225592157249, 8090.118728762442769,  
8515.514233243611457,
```

```
8903.736217784391415, 9490.83453915640887,  
10113.92888505620507}  
Do[beta[n]=b[[n]],{n,nterm}]
```

```
A1[n_]:=A1[n]  
Do[A1[n]=beta[n]/alpha1^0.5,{n,nterm}]
```

```
A2[n_]:=A2[n]  
Do[A2[n]=beta[n]/alpha2^0.5,{n,nterm}]
```

```
gam[n_]:=gam[n]  
Do[gam[n]=A1[n] L1,{n,nterm}]
```

```
et[n_]:=et[n]  
Do[et[n]=A2[n] L2,{n,nterm}]
```

```
aln=Table[0,{n,nterm}]  
Aln[n_]:=Aln[n]  
Do[Aln[n]=aln[[n]],{n,nterm}]
```

```
A2n[n_]:=A2n[n]  
Do[A2n[n]=(-h1*A1[n]*Sin[gam[n]]+Cos[gam[n]])*  
Sin[l*et[n]]-kk*al*Sin[gam[n]]*Cos[l*et[n]],  
{n,nterm}]  
a2n=Table[A2n[n],{n,nterm}]
```

```
b1n=Table[1,{n,nterm}]  
B1n[n_]:=B1n[n]  
Do[B1n[n]=b1n[[n]],{n,nterm}]
```

```
B2n[n_]:=B2n[n]  
Do[B2n[n]=kk*al*Sin[gam[n]]*Sin[l*et[n]]+  
(-h1*A1[n]*Sin[gam[n]]+Cos[gam[n]])*Cos[l*et[n]],  
{n,nterm}]  
b2n=Table[B2n[n],{n,nterm}]
```

```
Output from section: beta[n], Aln[n], B1n[n], A2n[n],  
B2n[n]
```

```

Define eigenfunctions Psi[section,x,n]

Define thermal diffusivity coefficient asection
=asection above

a[section_]:=a[section]
a[1]=6.7497*10^-08
a[2]=8.2079*10^-07

Define thermal conductivity ksection

k[section_]:=k[section]
k[1]=0.117
k[2]=2.1

Define thicknesses of layers L1,L2

L[section_]:=L[section]
L[1]=1.25*10^-6
L[2]=2.25*10^-6

Define Psi

Psi[section_,x_,n_]:=Psi[section,x,n]
Do[Psi[1,x,n]=A1n[n] Sin[beta[n] x/
Sqrt[a[1]]]+B1n[n] Cos[beta[n] x/
Sqrt[a[1]]],{n,1,nterm}]
Psi[1,x,2]
Do[Psi[2,x,n]=A2n[n] Sin[beta[n] x/
Sqrt[a[2]]]+B2n[n] Cos[beta[n] x/
Sqrt[a[2]]],{n,1,nterm}]
Psi[2,x,2]

Define dummy Psi for integration

Psip[section_,xp_,n_]:=Psip[section,xp,n]
Do[Psip[1,xp,n]=A1n[n] Sin[beta[n] xp/
Sqrt[a[1]]]+B1n[n] Cos[beta[n] xp/
Sqrt[a[1]]],{n,1,nterm}]
Psip[1,xp,2]
Do[Psip[2,xp,n]=A2n[n] Sin[beta[n] xp/
Sqrt[a[2]]]+B2n[n] Cos[beta[n] xp/
Sqrt[a[2]]],{n,1,nterm}]
Psip[2,xp,2]

Define Norm[n]

Norm[n_]:=Norm[n]
Do[Norm[n]=k[1]/a[1] Integrate[Psip[1,xp,n]^2,{xp,
0,L[1]}]+k[2]/a[2] Integrate[Psip[2,xp,n]^2,{xp,

```

```
L[1],L[2]},{n,nterm}]
Norm[5]
```

```
Define Green's Functions G[i,j,x,t,xp,tp,case]
```

```
G[i_,j_,x_,t_,xp_,tp_]:=G[i,j,x,t,xp,tp]
Do[G[i,j,x,t,xp,tp]=Sum[Exp[-beta[n]^2*(t-tp)]*
k[j]/a[j]/Norm[n]*Psi[i,x,n]*Psip[j,xp,n],
{n, nterm}],{i,2},{j,2}]
```

```
G[1,2,x,t,xp,tp]
```

```
G0[i_,j_,x_,t_,xp_,tp_]:=G0[i,j,x,t,xp,tp]
```

```
Do[G0[i,j,x,t,xp,0]=Sum[Exp[-beta[n]^2*(t-0)]*
k[j]/a[j]/Norm[n]*Psi[i,x,n]*Psip[j,xp,n],
{n, nterm}],{i,2},{j,2}]
```

```
G0[1,2,x,t,xp,0]
```

```
G0[1,1,x,t,xp,0]
```

```
G0[2,1,x,t,xp,0]
```

```
G0[2,2,x,t,xp,0]
```

```
Define Initial Temperature Distributions F1,F2 and
heat generation g
```

```
F[j_,xp_]:=F[j,xp]
```

```
F[1,xp]=0
```

```
F[2,xp]=0
```

```
g[j_,xp_,tp_]:=g[j,xp,tp]
```

```
g[1,xp,tp]=0
```

```
g[2,xp,tp]=5.5*10^13
```

```
Define Ti(x,t)
```

```
T[i_,x_,t_]:=T[i,x,t]
```

```
Do[T[i,x,t]=Tinf+
```

```
Integrate[G0[i,1,x,t,xp,0]*F[1,xp],{xp,0,L[1]}]+
```

```
Integrate[G0[i,2,x,t,xp,0]*F[2,xp],{xp,L[1],L[2]}]+
```

```
Integrate[G[i,1,x,t,xp,tp]*a[1]/k[1]*g[1,xp,tp],
```

```
{xp,0,L[1]},{tp,0,t}]+
```

```
Integrate[G[i,2,x,t,xp,tp]*a[2]/k[2]*g[2,xp,tp],
```

```
{xp,L[1],L[2]},{tp,0,t}],{i,2}]
```

```
TSect1=T[1,x,t]
```

```
TSect2=T[2,x,t]
```

```
g[1,xp,tp]
```

```
g[2,xp,tp]
```

A.3 Temperature Distribution Output Program

Temperature functions in x,t for PP (TPP) and Boehmite (TB)

```
TPP= ... from "h2c=∞ mod";
```

```
TB= ... from "h2c=∞ mod";
```

Definition of L1, L2

```
L1=1.25*10^-6;
```

```
L2=2.25*10^-6;
```

Temperature functions at the interface boundary for PP (TPPL1) and Boehmite (TBL1)

```
TPP;  
%/.x->L1;  
TPPL1=%;
```

```
TB;  
%/.x->L1;  
TBL1=%;
```

```
T250=250;
```

```
Plot[{TPPL1,TBL1,T250},{t,0,2*10^-5}]
```

-Graphics-

Estimated time until Boehmite at interface reaches 250° C

```
TBL1;  
%/.t->1.62069*10^-5
```

```
250.
```

```
TBL1;  
%/.t->1.62069*10^-5
```

```
250.
```

```
TB;  
%/.t->1.62069*10^-5;  
TBt=%;
```

```
TPP;  
%/.t->1.62069*10^-5;  
TPPt=%;
```

```
Show[Plot[TPPt,{x,0,L1},AxesOrigin->{0,0}],  
Plot[TBt,{x,L1,L2},AxesOrigin->{0,0}],  
Plot[150,{x,0,L1},AxesOrigin->  
>{0,0}],Plot[250,{x,L1,L2}],  
AxesOrigin->{0,0}]
```

-Graphics-

```
Show[Plot[TPPt,{x,0,L1},AxesOrigin->{0,0},  
DisplayFunction->Identity],  
Plot[TBt,{x,L1,L2},AxesOrigin->{0,0},  
DisplayFunction->Identity],  
Plot[150,{x, 0, L1},PlotStyle->Dashing[{0.05,0.05}],  
AxesOrigin->{0,0},DisplayFunction->Identity],  
Plot[250,{x, L1, L2},PlotStyle->Dashing[{0.05,0.05}],  
AxesOrigin->{0,0},DisplayFunction->Identity],  
DisplayFunction:>$DisplayFunction,AxesOrigin->{0,0},  
AxesLabel->{"x(s)","T(°C)"},Ticks->  
>{{0,L1,L2},Automatic},  
Axes->True]
```

Analysis at 14.5 ms

```
TB;  
%/.t->1.45*10^-5;  
TBt145=%;
```

```
TPP;  
%/.t->1.45*10^-5;  
TPPt145=%;
```

```
Show[Plot[TPPt145,{x,0,L1}],Plot[TBt145,{x,L1,L2}],  
Plot[150,{x,0,L1}],Plot[250,{x,L1,L2}]]
```

-Graphics-

```
TPPt145;  
%/.x->.599*L1
```

150.062

```
TPPt145;
```

```
%/.x->L1
```

```
229.271
```

```
TBt145;
```

```
%/.x->L1
```

```
229.271
```

Determine Temperature Distribution Within Boehmite When Interface Reaches 250° C

```
TPP;
```

```
%/.t->1.62069*10^-5;
```

```
TPPL1250=%;
```

```
T150=150
```

```
150
```

```
Plot[{TPPL1250,T150,125},{x,0,L1},PlotRange->{0,250}]
```

-Graphics-

86.84 % of Polypropylene (2.18 of 2.5 micrometers) under 150° C

82.83 % of Polypropylene (2.08 of 2.5 micrometers) under 125° C

```
TPPL1250;
```

```
%/.x->.451*L1
```

```
150.053
```

```
TPPL1250;
```

```
%/.x->.19*L1
```

```
129.237
```

```
.8726*L1*2
```

```
.83347*L1*2
```

```
2.1815 10-6
```

```
2.08368 10-6
```

B. Finite Difference Model - Fortran code

B.1 Input file - hyp.in

```
121 81 3000 2.5d-06 3.5d-06 1.0d-08
0.5d0 2.5d+01 0.0d+06 5.5d+13 0.0001d+00
10 0.30
c npt1/npt2/ntime/r1/r2/dt
c lam/t0/qdot1/qdot2/hc
c nwrite/fomax
```

B.2 Executable file - hyp.f

```
program hyp
c
c Research finite difference model
c Infinite contact conductance check
c Polypropylene fiber coated with boehmite
c
implicit double precision(a-h,o-z)
double precision lam,l1,k1,k2
common/ props/ r1,r2,qdot,hc,k1,k2
parameter(is=200)
dimension a(is),b(is),c(is),rhs(is),t(is),tp(is)
data k1,ro1,cp1/ 1.17d-1,9.d02,1.926d3/
data k2,ro2,cp2/ 2.1d0,3.01d3,8.5d2/
open(1,file='hyp.in')
open(2,file='hyp.out')
read(1,*)npt1,npt2,ntime,r1,r2,dt
read(1,*)lam,t0,qdot1,qdot2,hc
read(1,*)nwrite,fomax
l1=1.d0-lam
npts=npt1+npt2-1
dr1=r1/ dble(npt1-1)
dr2=(r2-r1)/ dble(npt2-1)
alph1=k1/(ro1*cp1)
alph2=k2/(ro2*cp2)
fo1=alph1*dt/dr1**2
fo2=alph2*dt/dr2**2
```

```

bi=hc*dr2/k2
c
c ... set up coefficient matrix
c
rr=0.0d0
fo=fo1
c
c ... center node
b(1)=1.d0+4.d0*fo*lam
c(1)=-4.d0*lam*fo
c
c ... nodes in wire
do 10 i=2,npt1-1
rr=rr+dr1
gp=1.d0+dr1/(2.d0*rr)
gm=1.d0-dr1/(2.d0*rr)
a(i)=-lam*gm*fo
b(i)=(1.d0+2.d0*lam*fo)
c(i)=-lam*gp*fo
10 continue
c
c ... interface node
fo1b=2.d0*k1*dt/(ro1*cp1*dr1+ro2*cp2*dr2)/dr1
fo2b=fo1b*(dr1/dr2)*(k2/k1)
gp=1.d0+dr2/(2.d0*r1)
gm=1.d0-dr1/(2.d0*r1)
a(npt1)=-lam*gm*fo1b
b(npt1)=1.d0+lam*(fo1b*gm+fo2b*gp)
c(npt1)=-lam*gp*fo2b
c
c ... nodes in insulation
fo=fo2
rr=r1
do 12 i=npt1+1,npt1+npt2-2
rr=rr+dr2
gp=1.d0+dr2/(2.d0*rr)
gm=1.d0-dr2/(2.d0*rr)
a(i)=-lam*gm*fo
b(i)=(1.d0+2.d0*lam*fo)
c(i)=-lam*gp*fo
12 continue
c
c ... convection at surface

```

```

gm=1.d0-dr2/r2/2.d0
a(npt1+npt2-1)=-2.d0*gm*fo*lam
b(npt1+npt2-1)=1.d0+2.d0*fo*lam*(gm+bi)
c
c ...set initial temps
c
do 15 i=1,npts
  t(i)=0.0d0
  tp(i)=0.0d0
15 continue
iwrite=0
l1=1.d0-lam
do 40 itime=1,ntime
  iwrite=iwrite+1
do 18 i=1,npts
18 t(i)=tp(i)
  time=dbl(itime)*dt
  fo=fo1
  rhs(1)=(1.d0-4.d0*l1*fo)*t(1)+4.d0*l1*fo*t(2)
  2   +qdot1*alph1*dt/k1
  rr=0.0d0
do 20 i=2,npt1-1
  rr=rr+dr1
  gp=1.d0+dr1/(2.d0*rr)
  gm=1.d0-dr1/(2.d0*rr)
  rhs(i)=l1*fo*gm*t(i-1)+(1.d0-2.d0*l1*fo)*t(i)
  2   +l1*fo*gp*t(i+1)+qdot1*alph1*dt/k1
20 continue
gp=1.d0+dr2/(2.d0*r1)
gm=1.d0-dr1/(2.d0*r1)
rhs(npt1)=l1*fo1b*gm*t(npt1-1)
  2   +(1.d0-l1*(fo1b*gm+fo2b*gp))*t(npt1)
  3   +l1*fo2b*gp*t(npt1+1)
  4   +qdot1*fo1b*(dr1**2/k1/2.d0)
  5   +qdot2*fo2b*(dr2**2/k2/2.d0)
fo=fo2
rr=r1
do 21 i=npt1+1,npt1+npt2-2
  rr=rr+dr1
  gp=1.d0+dr2/(2.d0*rr)
  gm=1.d0-dr2/(2.d0*rr)
  rhs(i)=l1*fo*gm*t(i-1)+(1.d0-2.d0*l1*fo)*t(i)
  2   +l1*fo*gp*t(i+1)+qdot2*alph2*dt/k2

```

```

21 continue
   gm=1.d0-dr2/(2.d0*r2)
   rhs(npts)=2.d0*gm*11*fo*t(npts-1)
2   +(1.d0-2.d0*11*fo*(gm+bi))*t(npts)
3   +qdot2*alph2*dt/k2
c 22 write(2,101)i,a(i),b(i),c(i),rhs(i)
101 format(3x,i3,2x,d12.5,1x,d12.5,1x,d12.5,3x,d12.5)
   ll=1
   call tridag(ll,npts,is,a,b,c,rhs,tp)
   nout=dbl(iwrite/nwrite)
   if(nout.gt.0)then
   write(2,203)time
   rr=-dr1
   do 24 i=1,npts
   if(i.le.npt1)then
   dr=dr1
   else
   dr=dr2
   endif
   rr=rr+dr
   write(2,202)rr/r2,tp(i)+t0
24 continue
202 format(5x,f6.4,3x,f12.2)
203 format(/,4x,'time = ',f9.8)
   iwrite=0
   endif
40 continue
   stop
102 format(5x,i3,f7.3)
103 format(/,2x,'time = ',f6.2)
104 format(1x,f6.1,2x,15(f4.1,1x))
   end

```

c

=====

====

```

subroutine tridag(if,l,is,a,b,c,d,v)
implicit double precision(a-h,o-z)
dimension a(is),b(is),c(is),d(is),v(is),beta(500),gamma(500)

```

c

```

beta(if)=b(if)
gamma(if)=d(if)/beta(if)
ifp1=if+1

```

c

```

do 1 i=ifp1,l
  beta(i)=b(i)-a(i)*c(i-1)/beta(i-1)
1  gamma(i)=(d(i)-a(i)*gamma(i-1))/beta(i)
c
  v(l)=gamma(l)
  last=l-if
  do 2 k=1,last
    i=l-k
2  v(i)=gamma(i)-c(i)*v(i+1)/beta(i)
c
  return
end

```

Vita

The author, Daniel Bernard Skinner, was born on November 28, 1969 in Wilmington, DE. He lived in Newark, DE and graduated from Newark High School in 1988. He completed his undergraduate studies at the University of Delaware in May of 1993, earning a Bachelor of Mechanical Engineering Degree with a Minor in Business Administration. He then enrolled at Virginia Polytechnic Institute and State University, earning a Master of Science Degree in Mechanical Engineering in November 1995.